NPL

National Physical Laboratory

Good Practice Guide No. 87

Prediction of the impact performance of plastics using finite element methods

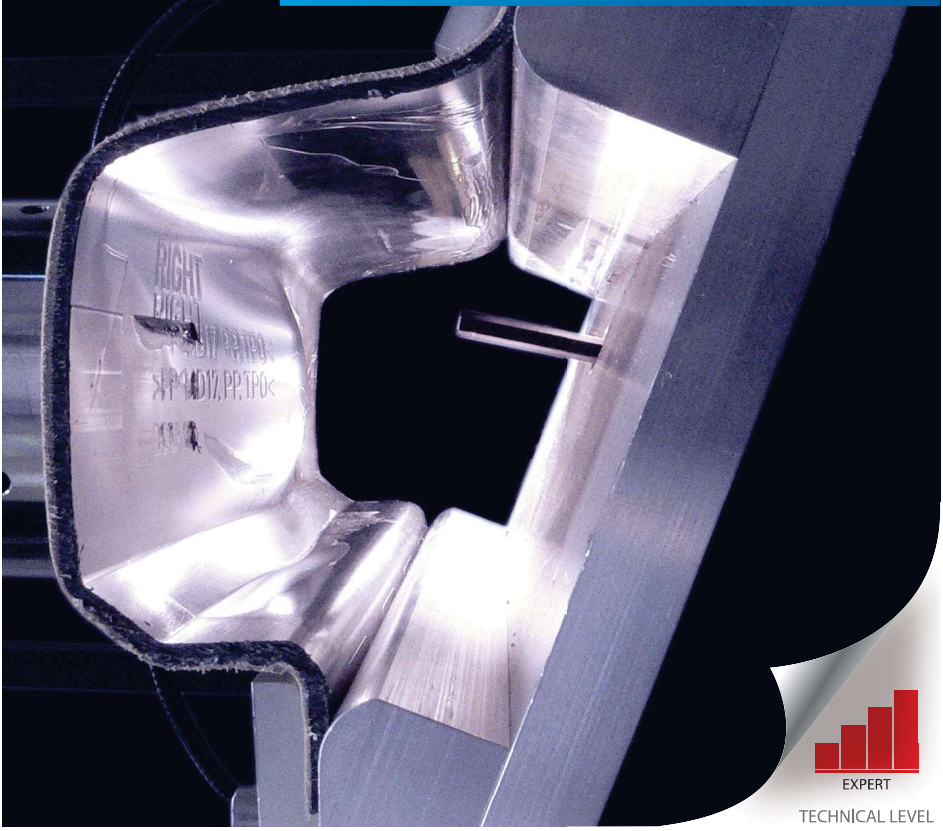

EXPERT

TECHNICAL LEVEL

Department for Business, Energy & Industrial Strategy

FUNDED BY BEIS

The National Physical Laboratory (NPL)

NPL is the UK's National Measurement Institute, and is a world-leading centre of excellence in developing and applying the most accurate measurement standards, science and technology available.

NPL's mission is to provide the measurement capability that underpins the UK's prosperity and quality of life.

Version 1.0

NPL Authors and Contributors

Greg Dean
Louise Crocker

Find out more about NPL measurement training at **www.npl.co.uk/training** or our e-learning Training Programme at **www.npl.co.uk/e-learning**

National Physical Laboratory
Hampton Road
Teddington
Middlesex
TW11 0LW
United Kingdom

Telephone: +44 (0)20 8977 3222
e-mail: training@npl.co.uk
www.npl.co.uk

Abstract/Foreword

This Guide describes the application of Finite Element Analysis (FEA) for predicting the impact performance of plastics and the measurement of input data. Two elastic-plastic materials models are presented that are able to describe the large strain, non-linear behaviour of plastics when this is caused by yield and flow. These models are the von Mises and linear Drucker-Prager models available in finite element (FE) packages. An additional model is also introduced as an example of a bespoke user defined model. This model takes account of the influence of cavitation on plastic deformation.

Test methods are described for the determination of property data and parameters required by these models for the simulation of impact performance using finite element methods. The determination of properties at high strain rates is achieved by modelling measurements at low and moderate strain rates and calculating the behaviour at high strain rates by extrapolation.

The basics of setting up an FE analysis for modelling impact are discussed within this guide, covering topics such as element selection; analysis type; selection of material model and model parameter sensitivity. Examples from impact analyses of door trim subcomponents are used to illustrate the pertinent points.

Acknowledgements

This Guide was originally produced in 2006 within the *Modelling the behaviour of plastics for design under impact* project, part of the *Measurement for Materials Processing and Performance* programme sponsored by the National Measurement System Directorate of the Department of Trade and Industry. The authors acknowledge the contribution to this work by F. Dunne (originally at Oxford University, now at Imperial College London) with writing the code to enable the cavitation model to be used with the Abaqus finite element system. The assistance is also acknowledged of L. Wright at NPL with the application of the cavitation model in Abaqus. The door trim mouldings were supplied by Jaguar Land Rover. Good Practice Guide No. 87 has been updated as part of a review of composite and adhesive GPGs within NPL's National Measurement System programme funded by BEIS.

Contents

Introduction 1

Introduction 2

Nomenclature 4

Materials Models 6

Deformation of ductile plastics 7

Elastic-plastic behaviour 8

Elastic behaviour 8

Plastic behaviour 8

Elastic-plastic models 9

The von Mises model 9

The linear Drucker-Prager model 10

The cavitation model 12

Measurement of properties required for FEA 15

General 16

Tensile tests 17

At low strains 17

At high strains 18

At high strain rates 21

Shear tests 22

Compression tests 23

Determination of model parameters 24

General 25

Tensile modulus and Poisson's ratio 25

Von Mises model parameters 26

Linear Drucker-Prager model parameters 27

Cavitation model parameters 29

Rate-dependent plasticity 32

General 32
Tensile behaviour 33
Shear behaviour 37
Rate-dependent elasticity 40
Application of Finite Element Analysis 44
FEA introduction and basics 45
Element type 46
EXAMPLE: Comparison of solid and shell elements 48
Mesh density 49
Contact surfaces and boundary conditions 50
Friction 51
EXAMPLE: Friction versus frictionless surface definitions 51
Choice of solver 53
EXAMPLE: Mass scaling in dynamic analyses 54
Precision level 55
EXAMPLE: Single versus double precision 56
Materials models 56
Material model selection 56
EXAMPLE: Comparison of elastic-plastic models 57
Rate-dependent behaviour 58
EXAMPLE: Comparison of single rate and rate-dependent analyses 58
Parameter sensitivity 60
EXAMPLE: Cavitation model parameter sensitivity 60
Predicting performance 63
EXAMPLE: Predicting deformation of the toptrim component 63
EXAMPLE: Optimisation of components 65
Conclusions 67
Conclusions 68
References 70
References 71

Chapter 1

Introduction

- Introduction
- Nomenclature

Introduction

Tough plastics have properties that make them particularly suited to applications where accidental impact loading is possible, and the material must withstand this without failure or must limit the force level sustained by other objects in the impact event. These applications include housings for domestic and electronic appliances, structural packaging and personal protection equipment. In particular, plastics are used for many components in motor vehicles that may be impacted by passengers or pedestrians in a road accident. Ideally, these components should minimise damage to the human body part involved in the impact. The ability to confidently predict the response of a plastics product under impact loading is therefore an important aspect of the design of these products in order to optimise safety and reliability in their performance.

A finite element analysis is a very powerful method for simulating the performance of a product under impact loading. Force deformation levels generated by the impact can be predicted as well as stress and strain distributions in the components involved. Where polymeric materials are involved, the high toughness of these materials can lead to the development of large strains through plastic deformation prior to failure. In order to obtain reliable predictions in an impact analysis, it is necessary to take proper account of the non-linear and strain-rate dependent behaviour of the polymer through use of a valid materials model.

In a finite element an array of 2- or 3-dimensional elements is used to define the shape and size of the components. A materials model is needed to describe the deformation behaviour of each material in the analysis. As with many predictive methods, the accuracy of results will depend on the suitability of the materials model selected for describing the deformation behaviour of the materials involved and the accuracy in the determination of property data required by the model. Under impact loading, a tough polymer may be subjected to large strains involving yielding and plastic flow before rupture. Elastic-plastic models are used in finite element systems to describe large strain, non-linear behaviour under these circumstances. These models employ a yield criterion and a flow law to calculate components of stress and strain under conditions where the deformation behaviour is non-linear.

The elastic-plastic models generally available in finite element systems were developed for metals and some other materials, and their validity for a wide range of plastics is uncertain. In particular, there is an important class of plastics that undergo cavitation in microscopic regions of the polymer under stress states and stress levels where there is a dilatational component of stress that is sufficient to nucleate the cavities. Cavitation is usually visible as stress whitening and is responsible for increased toughness by promoting localised shear yielding in the material between cavities. It will therefore lower the yield stress under those stress states for which the hydrostatic stress component is sufficient to cause cavitation. In rubber-toughened plastics [1], the rubber particles have been introduced to improve toughness and are sites for

cavity nucleation. In semi-crystalline polymers where the amorphous phase is rubbery, such as the polyethylenes and polypropylenes at ambient temperatures, the sites of cavitation are the amorphous regions between crystallites.

Experimental methods for measuring the properties required by these models are not routine and have not been fully standardised. At small strains, behaviour is linear viscoelastic, which can complicate the determination of a value for tensile modulus. At higher strains, an increasing proportion of the deformation is plastic, and at strain levels above the peak in stress in tensile tests, the use of standard specimen geometries [2] is not appropriate because the strain distribution in the gauge region of the specimen is not uniform. In addition, measurements of Poisson's ratio over a wide range of strain are needed for the calculation of true stresses. For the determination of the parameters for some elastic-plastic models, stress/strain measurements are required under more than one stress state. Tensile tests are relatively straightforward, but data are also needed under other stress states such as shear and compression. Furthermore, to achieve acceptable accuracy in predictions of performance under impact, it is necessary to take account of the dependence of properties on strain rate. Measurements of stress/strain curves at the high strain rates associated with impact events are difficult because of the high test speeds and are subject to errors arising from problems with the measurement of strain and from resonance and transient vibrations in the force transducer, test specimen and test assembly.

In this Good Practice Guide, two elastic-plastic models that are commonly available in finite element systems are introduced, and their application to plastics materials is illustrated using experimental data on a tough polymer used in motor vehicle interiors. The test methods used to obtain the data are described, and the analysis of these data is explained to derive the parameters in each model. The determination of properties at high strain rates associated with impact events is difficult experimentally because of problems with transient forces and with strain measurements at high speeds. A procedure is described for obtaining these data by modelling results at lower speeds and calculating properties at high strain rates by extrapolation. The limitations of some models used in finite element analyses for predicting the large deformation behaviour of materials in situations where numerous small cavities form at elevated strains is illustrated. In many FE packages there is often the opportunity to create bespoke user material models which can be used instead of the standard models provided by the packages. In this guide, the use of an alternative model is demonstrated. This cavitation model was developed over a number of years to take account of the influence of cavitation on plastic deformation.

The application of finite element analyses to modelling impact is discussed within this guide. This includes the basics of setting up an analysis, such as element selection, analysis type and selection of material model. For reliable predictions, accurate materials parameters must be used. Results are presented of a small study carried out to indicate how sensitive the predictions are to parameter changes in the cavitation model, which requires a large number

of input parameters. Examples from impact analyses of door trim subcomponents using parameters obtained on a rubber-toughened propylene copolymer are used to illustrate the pertinent points.

Nomenclature

Definitions of all symbols appearing in this guide are provided below.

σ_i, ε_i	components of principal stress and strain respectively (i = 1,2 and 3)
σ', ε'	engineering values of stress and strain respectively
σ'_T, ε'_T	engineering values of stress and strain respectively under tension
ε'_t	engineering value of transverse strain
σ, ε	true values of stress and strain respectively
ε_T, ε_S	true values of strain under tension and shear respectively
ε^e, ε^p	true values of the elastic and plastic components of strain respectively
ε_t^e, ε_t^p	true elastic and plastic components of transverse strain under uniaxial tension or compression
σ_T, σ_S, σ_C	true stresses under tension, shear and compression respectively
ε_T^p, ε_S^p, ε_C^p	true plastic strains under tension, shear and compression respectively
$\dot{\varepsilon}$, $\dot{\varepsilon}_T^p$	strain rate and tensile plastic strain rate respectively
σ_e, q	the effective shear component of stress
σ_o, ε_o^p	effective shear yield stress and plastic strain respectively
σ_m, -p	the hydrostatic component of stress
E, G	tensile modulus and shear modulus respectively
ν'	Poisson's ratio calculated from engineering strains
ν	Poisson's ratio calculated from true strains
ν^e	the elastic component of Poisson's ratio
ν^p	the plastic components of Poisson's ratio
μ, β	hydrostatic stress sensitivity parameters in the linear Drucker-Prager yield criterion

F	the flow potential
μ', Ψ	parameters in the flow potential for non-associated flow
f	volume fraction of cavities
σ_M	yield stress of the matrix material between cavities in a rubber-toughened polymer
v_C	volume fraction of cavities when cavitation is complete
q_1	cavitation interaction parameter
μ_1'	parameter to indicate when cavitation is complete
ε_{1V}, ε_{2V}, β	parameters in the cavity nucleation criterion
k	parameter that relates yield stress to the volume fraction of the cavitating phase v_C
σ_f, σ_i, ε_a, n,	parameters in a function used to model plastic strain hardening in tension
σ_{of}, σ_{oi}, ε_{oa}, n_o	parameters in a function used to model plastic strain hardening in shear
σ_{fo}, A	parameters in an equation used to model rate-dependent plasticity in tension
σ_{ao}, B	parameters in an equation used to model rate-dependent plasticity in tension
σ_{ofo}, C	parameters in an equation used to model rate-dependent plasticity in shear

Chapter 2

Materials Models

- Deformation of ductile plastics
- Elastic-plastic behaviour
- Elastic-plastic models

Deformation of ductile plastics

Most engineering plastics are tough materials that can undergo extensive deformation involving yielding and plastic flow before failure. A typical plot of stress against strain for such a material is shown in Figure 1 generated by a test carried out at constant deformation rate. At small strains, behaviour is predominantly linear elastic. More precisely, the behaviour here is linear viscoelastic which implies that the stress/strain relationship will be curved. The curvature arises because of stress relaxation in the polymer during the test, and the amount of curvature will depend on the relaxation times of the molecular motions giving rise to viscoelasticity. The influence of viscoelasticity on the stress/strain relationship under constant strain rate is described further in Chapter 4.

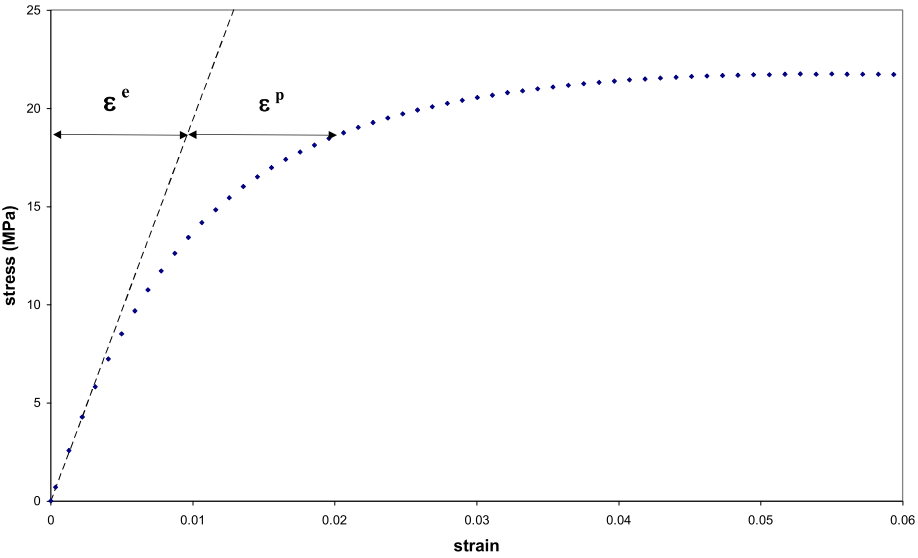

Figure 1. *The determination of elastic and plastic components of strain from a stress vs strain curve.*

At higher strains, behaviour becomes non-linear. This is associated with enhanced stress relaxation or creep in the polymer caused by an increase in molecular mobility induced by the elevated stresses. Although much of the deformation is recoverable at moderate strain levels, at higher strains the deformation becomes increasingly dominated by yielding and plastic flow. Satisfactory models for non-linear viscoelasticity have yet to be developed, and most finite element packages describe non-linear behaviour in terms of elastic-plastic models which were developed for metals and adapted for use with other materials.

Elastic-plastic behaviour

Elastic behaviour

With elastic-plastic models, calculations of stress and strain distributions at low strains are based on linear elasticity. Because it is generally more accurate to measure properties using tensile tests, linear elastic behaviour is usually characterised by values for the tensile modulus E and the elastic Poisson's ratio ν_e.

Plastic behaviour

The onset of non-linearity in stress/strain behaviour in elastic-plastic models is ascribed to plastic deformation and occurs at a stress level regarded as the first yield stress. The subsequent increase in stress with strain is associated with the effects of strain hardening. In this non-linear region, the total strain ε is considered to be the sum of a recoverable elastic component ε^e and a plastic component, ε^p as illustrated in Figure 1. Thus

$$\varepsilon = \varepsilon^e + \varepsilon^p \tag{1}$$

The hardening behaviour is required for the stress analysis and is most commonly described by a plot of the tensile yield stress σ_T against the tensile plastic strain ε_T^p which is referred to as the tensile hardening curve or hardening function. From equation (1) , plastic strain components in tension are given by

$$\varepsilon_T^p = \varepsilon_T - \frac{\sigma_T}{E} \tag{2}$$

Analogous equations exist for plastic strain components in shear and compression (see Chapter 4).

Tensile stress and strain components defining the hardening curve, σ_T and ε_T^p, are usually required by the FE analysis to be true values. Engineering values of stress and strain σ'_T and ε'_T are derived using the unstrained specimen dimensions and are related to true values by the equations

$$\sigma_T = \frac{\sigma'_T}{(1 - \nu'\varepsilon'_T)^2} \tag{3}$$

and

$$\varepsilon_T = \ln(1 + \varepsilon'_T) \tag{4}$$

Here ν' is the engineering Poisson's ratio given by

$$\nu' = -\frac{\varepsilon'_t}{\varepsilon'_T} \tag{5}$$

where ε'_t is the engineering transverse strain and is negative in a tensile test. Note that under uniaxial compression, ε'_t is positive whilst the compressive strain ε'_C is negative. Relationships for the true Poisson's ratio and the plastic component of Poisson's ratio are given by equations similar to equation (5) but with appropriate components of transverse and axial strain.

Stress analysis calculations involve the use of multiaxial yield criteria and a flow law, and some of the yield criteria that have been used to model deformation in plastics are described in the following sections. The yield criterion relates components of applied stress field to material parameters after the onset of yielding.

The calculation of plastic strain components is achieved in plasticity theory using a flow rule (for example see equations (17) and (18) for the linear Drucker-prager model), which relates increments of plastic strain to a plastic flow potential. If the flow behaviour for a particular material is such that the flow potential can be identified with the yield function then this is termed associated flow. In general, this will be an approximation and the extra information needed to characterise non-associated flow is described in the next section.

Elastic-plastic models

The von Mises model

The most simple yield criterion interprets yielding as a purely shear deformation process that occurs when the effective shear stress σ_e reaches a critical value [3, 4]. This effective stress is defined in terms of principal stress components σ_i (i = 1, 2 or 3) by

$$\sigma_e = \left\{\frac{1}{2}[(\sigma_1 - \sigma_2)^2 + (\sigma_2 - \sigma_3)^2 + (\sigma_3 - \sigma_1)^2]\right\}^{1/2} \tag{6}$$

The von Mises criterion then relates σ_e to the yield stress in tension σ_T by

$$\sigma_e = \sigma_T \quad (7)$$

Tensile yield stresses σ_T are material parameters and the minimum value denotes the limit of elastic behaviour and the start of plastic deformation. The increase in σ_T with tensile plastic strain ε_T^p is characterised by the hardening function. The von Mises criterion predicts that the tensile yield stress, shear yield stress σ_S and compressive yield stress σ_C are related by

$$\sigma_T = \sigma_C = \sqrt{3}\sigma_S \quad (8)$$

In this model, plastic deformation takes place under constant volume so the plastic component of Poisson's ratio is 0.5 and the flow parameter is zero. Tests on plastics under additional stress states such as shear and compression reveal that this relationship is not true because yielding is sensitive to the hydrostatic component of stress in addition to the shear component. Alternative criteria are considered in the next sections.

The linear Drucker-Prager model

Yielding in polymers is known to be sensitive to the hydrostatic component of stress as well as the shear component [3, 4]. Equation (7) can be extended to include hydrostatic stress sensitivity as follows

$$\sigma_e + \mu\sigma_m = \sigma_o \quad (9)$$

where σ_o is an effective shear yield stress $(= \sqrt{3}\sigma_S)$ and σ_m is the hydrostatic component of stress given by

$$\sigma_m = \frac{1}{3}(\sigma_1 + \sigma_2 + \sigma_3) \quad (10)$$

The material parameter μ determines the sensitivity of yielding to hydrostatic stress.

Equation (9) is identical to the linear Drucker-Prager model in the finite element package Abaqus [5] where the notation used is

$$t - p\tan\beta = d \quad (11)$$

where $t = \sigma_e$, $p = -\sigma_m$, $\tan\beta = \mu$ and $d = \sigma_o$. β is termed the friction angle.

A value for the material parameter μ can be determined from tests under two different stress states, and procedures for this are described in Chapter 4. According to the linear Drucker-Prager criterion, equation (9), equivalent stresses σ_S and σ_T are related by the expression

$$\sqrt{3}\sigma_S = \frac{(\mu + 3)}{3}\,\sigma_T \tag{12}$$

which gives

$$\mu = 3\left[\left(\sqrt{3}\,\sigma_S/\sigma_T\right) - 1\right] \tag{13}$$

where equivalent stresses σ_S and σ_T satisfy the equation

$$\sigma_T \varepsilon_T^p = \sigma_S \varepsilon_S^p \tag{14}$$

There are corresponding expressions for different combinations of data:

$$\mu = 3\left[1 - \left(\sqrt{3}\sigma_S/\sigma_C\right)\right] \tag{15}$$

from shear and compression data, and

$$\mu = \frac{3[(\sigma_C/\sigma_T) - 1]}{[(\sigma_C/\sigma_T) + 1]} \tag{16}$$

from compression and tension data.

It should be noted that the above yield stresses σ_C, σ_T and σ_S in equations (15) and (16) are associated with the same plastic work (similar to equation (14)).

The flow rule is used in elastic-plastic models for the determination of plastic strains through identification of a flow potential F. The most general form for the flow potential in the linear Drucker-Prager model is given by

$$F = \sigma_e + \mu'\sigma_m \tag{17}$$

The flow parameter μ' is a material property that differs from the value of μ in equation (9) if the polymer exhibits non-associated flow. It can be determined from measurement of the plastic component of Poisson's ratio ν^p using the expression

$$\mu' = \frac{3(1-2\nu^p)}{2(1+\nu^p)} \tag{18}$$

A value for ν^p can be calculated from Poisson's ratio versus strain data using the equation

$$\nu^p = \frac{\nu\,\varepsilon_T - \nu^e\,\sigma/E}{\varepsilon_T - \sigma/E} \tag{19}$$

In Abaqus, the flow potential, G, is expressed in the form

$$G = t - p\tan\Psi \tag{20}$$

where tan ψ has replaced μ'. ψ is termed the dilation angle.

The cavitation model

The linear Drucker-Prager model described above is more complex and gives an improvement over the von Mises model by taking account of the influence of the hydrostatic component of stress on yield behaviour. For certain types of polymer this model still has some limitations. In these materials the yield behaviour under tension is very different from that under compression or shear because of the nucleation of numerous small cavities in the polymer under stress. This is usually visible as stress whitening. In rubber-toughened plastics, the rubber particles are sites for cavity nucleation. In semi-crystalline polymers where the amorphous phase is rubbery, such as polyethylenes and polypropylenes at ambient temperatures, the sites of cavitation are the amorphous regions between crystallites. Cavity nucleation improves the toughness of the polymer by promoting localised but widespread shear yielding in the matrix material between cavities. It will therefore lower the yield stress under those stress states for which the hydrostatic stress component is sufficient to cause cavitation.

In FE packages there is often the opportunity to create user material models which can be used instead of the standard models provided by the packages. As an example of this, a cavitation model, developed at NPL over a number of years [6, 7] to take account of the influence of cavitation on plastic deformation, is described below.

In the absence of cavitation, equation (9) is a satisfactory criterion for yielding. This equation has been modified to include the effects of cavitation as follows [8-11]

$$\frac{\sigma_e^2}{\sigma_M^2} - (q_1 f)^2 + 2q_1 f \cosh \frac{3\sigma_m}{2\sigma_M} = \left(1 - \frac{\mu\sigma_m}{\sigma_M}\right)^2 \quad (21)$$

Here f is the effective volume fraction of cavities which at small strains is zero but increases over some characteristic strain region associated with cavity nucleation. Neglecting cavity growth, the maximum value for f is v_C and occurs when cavity nucleation is complete. The value for v_C in semi-crystalline polymers will be associated with the volume fraction of the amorphous phase but might be expected to vary with molecular orientation. In rubber-toughened, glassy polymers, v_C can be identified with the volume fraction of rubber.

The parameter q_1 has been introduced [9] to account for the effect of void interactions on the stress distribution in the matrix between cavities. σ_M is the effective yield stress of the matrix polymer between cavities and is equal to σ_o in the absence of cavities. As cavity nucleation proceeds and the rubbery regions become replaced by cavities, σ_M will increase with f. The relationship between σ_M and f will depend upon how the effective shear yield stress of the uncavitated polymer σ_o varies with the volume fraction v_C of the cavitatable phase. The results of experiments and model calculations on an unfilled propylene-ethylene copolymer [12] suggest that the yield criterion takes the form

$$\sigma_o = \sigma_{MC} \exp(-k v_C) \quad (22)$$

where σ_{MC} is the effective shear yield stress of the material between cavities when cavitation is complete.

The nucleation of a cavity is assumed to occur at some critical volumetric strain that varies with the size of the cavitatable region. For a distribution of sizes of these regions, the cavity nucleation should occur over a range of total volumetric strain ε_V.

The flow potential in this model is, by analogy with equation (17), assumed to be

$$F = \frac{\sigma_e^2}{\sigma_M^2} - (q_1 f)^2 + 2q_1 f \cosh \frac{3\sigma_m}{2\sigma_M} - \left(1 - \frac{\mu' \sigma_m}{\sigma_M}\right)^2 \quad (23)$$

The results of measurements of Poisson's ratio prior to cavity nucleation in tension and under uniaxial compression (where effective volume fraction of cavities, f = 0) indicate that μ' has a relatively low value when f = 0 which then increases with the cavity volume fraction. This observation has led to the following proposed expression for μ'

$$\mu' = \mu_1' \frac{(1 - v_C)}{(1 - f)} \tag{24}$$

where μ_1' is the value when cavitation is complete.

Chapter 3

Measurement of properties required for FEA

- General
- Tensile tests
- Shear tests
- Compression tests

General

The data requirements for simulating the impact performance of a component using finite element methods depend on the choice of materials model used to describe the deformation behaviour of the polymer as well as any approximating assumptions, such as whether material properties depend on strain rate. In general, the more complex the material model, the greater number of parameters required. For an analysis based on the von Mises yield criterion, data obtained from tensile tests are sufficient. With the linear Drucker-Prager model, additional data are needed from tests under a different stress state such as shear or compression. Results for the variation of Poisson's ratio with tensile strain are also needed. For the determination of all the parameters in the NPL cavitation model, measurements of stress/strain behaviour are required in tension, shear and compression.

At NPL, test methods and procedures for the analysis of test data have been developed to determine

- the tensile modulus and Poisson's ratio
- the variation of Poisson's ratio with strain out to large strains
- true stress/true strain curves in tension out to large strains
- stress/strain curves in shear
- true stress/true strain behaviour under uniaxial compression
- the variation of tensile stress/strain behaviour with strain rate

Brief descriptions of the test methods will be given in the remainder of this section together with references to where more detailed information can be found. Some illustrative results from these tests will be presented on a rubber-toughened, propylene-ethylene copolymer. The material was produced by Dow Plastics under the identification code dtf 1600. The polymer has been developed for enhanced impact performance and contains some talc filler. Injection moulded specimens were kindly supplied by Dow in the form of standard tensile specimens and square plates of width 80 mm.

The analysis of test results on these specimens to obtain the parameters required by different models is described in Chapter 4. Procedures for determining the rate dependence of properties at high strain rates associated with impact events are also described in Chapter 4.

Tensile tests

At low strains

Engineering stress/strain curves in tension and Poisson's ratio can be measured using the procedure defined by the international standard ISO 527 [2]. This standard specifies the use of a standard specimen prepared by injection moulding. Tensile stress/strain data are shown in Figure 2 obtained at a testing speed of 1 mm/s which gives a strain rate around the peak in stress of 0.01 s^{-1}. Stresses and strains are true values derived using equations (3) and (4). Also shown are Poisson's ratio values obtained from simultaneous measurements of transverse strain using equation (5).

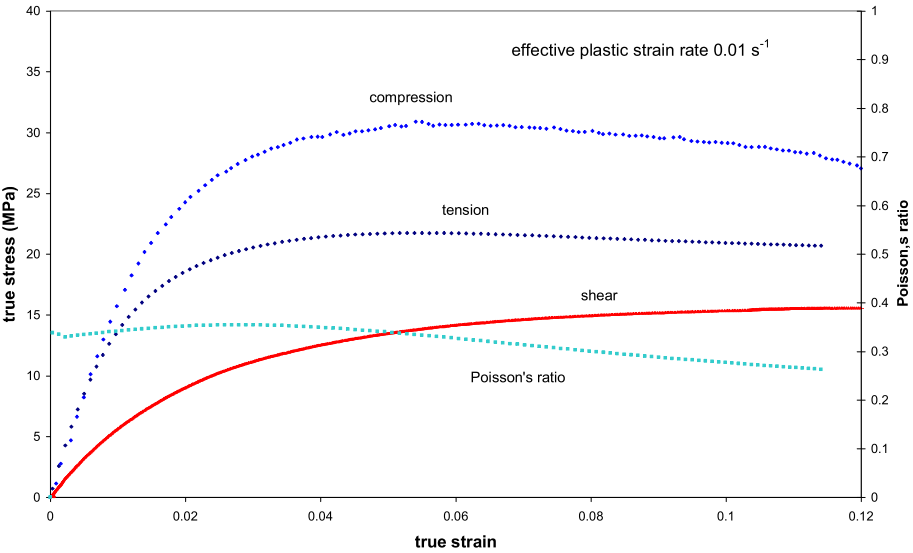

Figure 2. *Results from tests under tension, shear and compression made on injection moulded specimens.*

The ISO test is only suitable for the measurement of strain up to the peak in the stress/strain curve. At higher strains, the strain distribution in the parallel portion of the specimen is no longer uniform because of the onset of strain localisation. An alternative specimen geometry is then employed as described in the next section.

At high strains

Figure 3 shows results of tensile stress against tensile strain measurements on a single specimen of the rubber-toughened copolymer. The specimen geometry and dimensions were the same as the ISO tensile specimen [2]. Simultaneous strain measurements were made using a video extensometer in three separate regions of length 10 mm near the centre of the specimen. The results illustrate the distribution of strain that can occur in specimens of this geometry at strains above that corresponding to the peak in stress. The extent of the strain localisation depends on the flow behaviour of the polymer and hence the test temperature and speed. In extreme situations, the localisation is clearly visible through necking, but for many materials the extent of the non-uniformity in strain is less extreme and less apparent.

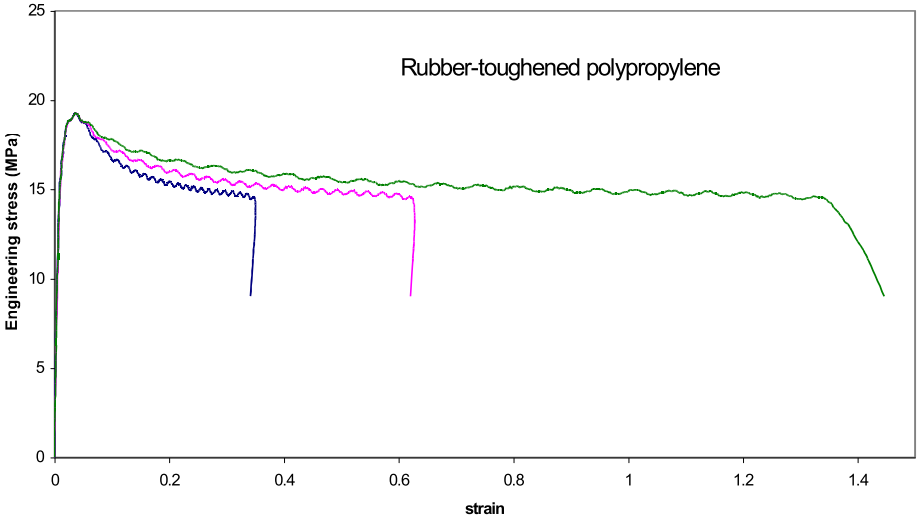

Figure 3. *Engineering stress/strain curves measured in a tensile test on a standard tensile specimen. A gauge length of 10 mm was used at 3 separate locations along the length of the specimen.*

In order to obtain more meaningful measurements of strain, and, in particular, of strain at failure, an alternative specimen geometry has been chosen that is illustrated in Figure 4. The waisted region is defined by a radius that locates the maximum stress, and hence onset of flow, at the centre of the specimen. The specimen can be conveniently machined from the central region of the ISO tensile specimen.

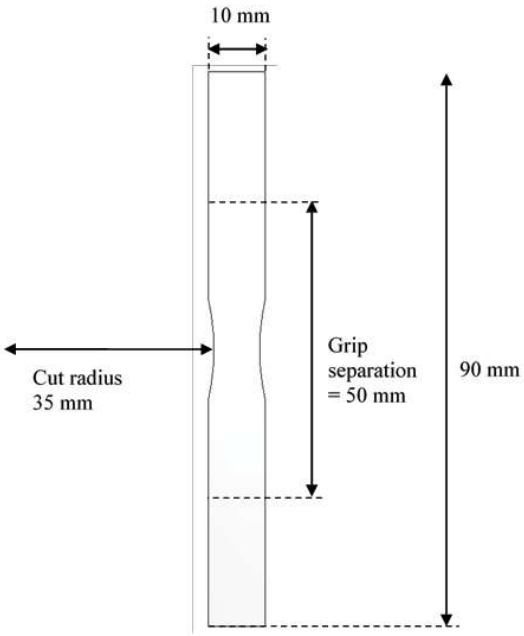

Figure 4. *Specimen geometry for the measurement of tensile behaviour at large strains.*

A finite element analysis has been used to calculate stress and strain distributions in the specimen under an applied load that was sufficient to cause plastic flow in the central region. The analysis took account of the dependence of plastic behaviour on strain rate (see Chapter 4). Calculated distributions of stress and strain in the specimen are shown in Figure 5 and reveal an essentially uniform stress and strain over a length of between 3 and 5 mm in the specimen centre. Extensometers (contacting and video) have therefore been used with a gauge length of 4 mm for the measurement of strain. Since this leads to significant uncertainties in the measurement of small strains (< 0.02), this specimen is used only for the determination of tensile behaviour at strains around and above the peak in stress

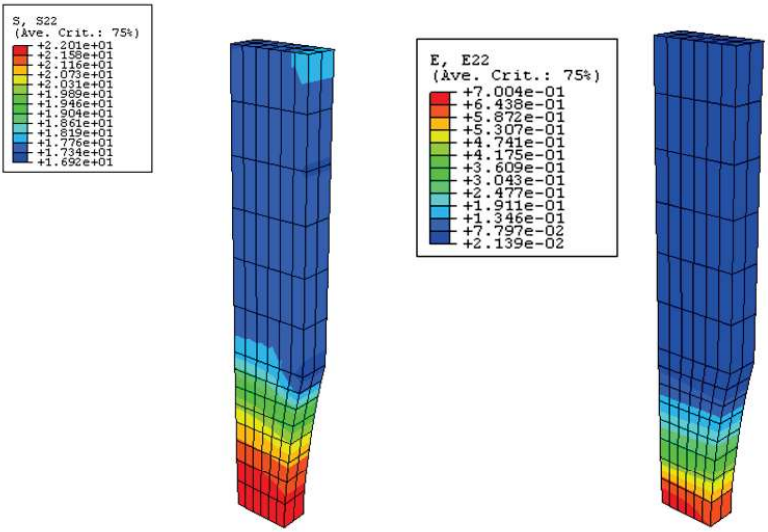

Figure 5. *Distributions of axial components of true stress and engineering strain in the waisted tensile specimen in Figure 4 calculated by FE analysis.*

This specimen is also used for the measurement of Poisson's ratio at moderate and high strains through simultaneous measurements of lateral strain in the width direction at the specimen centre and axial strain. This is believed to give more reliable results than the use of the standard specimen because of the greater precision in the determination of the axial strain at the location of the transverse strain measurement. It is worth noting however, that the finite element calculations reveal a slightly smaller transverse strain in the width direction at the specimen centre than in the thickness direction. This arises presumably because of some small constraint to free lateral contraction in the width direction owing to the onset of strain localisation in the waist. This suggests the use of a specimen with a more narrow waist to reduce the constraint, but this would lead to a reduced sensitivity in lateral strain measurement using a contacting extensometer to measure changes in specimen width. For the Poisson's ratio results reported here, no attempt has been made to correct for this source of error.

Figure 6 shows results for tensile stress and Poisson's ratio measurements with tensile strain obtained with this specimen geometry at a test speed of 0.1 mm/s. This speed is about 10 times lower than the speed used for the low strain measurements illustrated in Figure 2 yet the plastic strain rates in these tests are comparable at 0.01 s^{-1}. Figure 6 also shows values for true stress derived using the Poisson ratio measurements with equation (3).

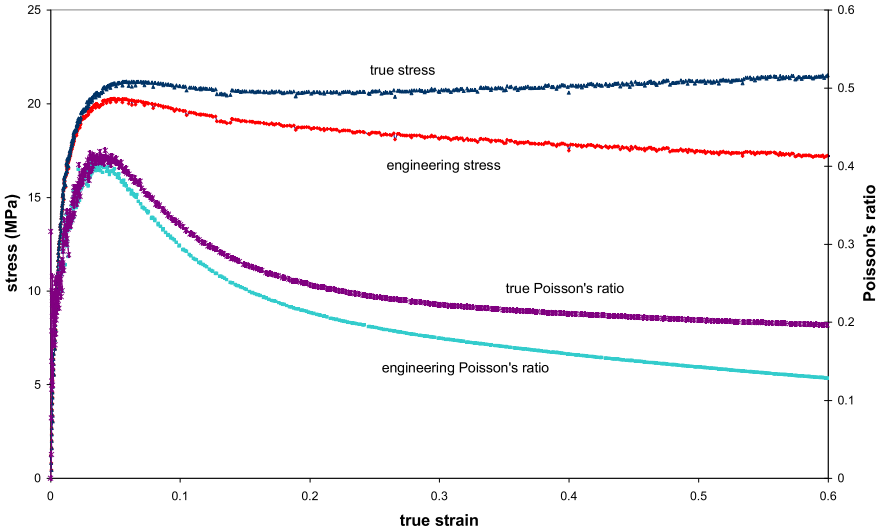

Figure 6. *Tensile results obtained on the waisted tensile specimen shown in Figure 4. Extensometer gauge length is 4 mm, test speed is 0.1 mm/s and strain rate is 0.01 s^{-1}.*

At high strain rates

The small waisted specimen geometry shown in Figure 4 can be used for the determination of tensile behaviour over a wide range of strain rate. For a given test speed, the strain rate in the central region of the specimen is significantly higher than obtained with the standard ISO specimen. Light-weight, contacting extensometers are used for axial strain measurement and are satisfactory at test speeds up to 100 mm/s where the strain rate in the gauge region is typically 10 s^{-1}. At this speed, errors in force measurement arising from resonances in the test assembly and wave effects in the specimen are generally negligible especially if components of low mass and high stiffness are used in the test assembly. The determination of properties at higher strain rates is achieved by modelling and extrapolation as described in Chapter 4.

Shear tests

Shear measurements can be carried out using a version of the test first proposed by Arcan et al [13]. The test specimen geometry and loading stages are shown in Figure 7. The test-piece geometry has been chosen so that a predominantly pure and uniform shear stress distribution is generated in the central region of the specimen.

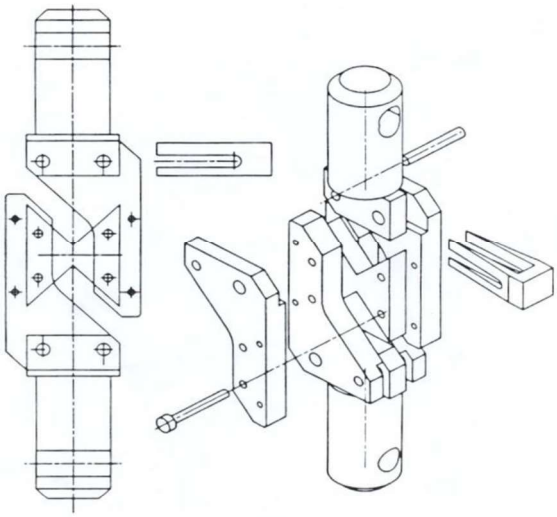

Figure 7. *Test assembly for the measurement of shear stress/strain curves using the notched plate method.*

The distance between the notches in the specimen is 12 mm and the notch radius is 1.5 mm. Shear strains are measured using a purpose-built extensometer that measures the relative displacement of points separated by a distance of 3 mm at the centre of the specimen. Shear stress/shear strain data obtained using this test on a specimen cut from an injection-moulded plate of the copolymer are shown with tensile data in Figure 2. In the calculation of shear stresses and strains, small corrections are applied for the non-uniform shear stress between the notches and for a contribution from bending to measured displacements A test speed of 10 mm/min was used giving a shear plastic strain rate of 0.02 s^{-1}. This gives an effective plastic strain rate (see equation (27) in Chapter 4) of about 0.01 s^{-1} which is comparable to the tensile data.

Compression tests

Compression measurements can be made on specimens with dimensions 10 mm x 10 mm with a thickness of 3mm minimum. The length and width dimensions are not critical. A larger length can be used, but, depending on the specimen thickness, buckling of the specimen will limit the strain at which useful data can be measured. On the other hand, a smaller length will reduce the accuracy in strain measurements and will increase the influence on results of the lateral constraint imposed on the loaded faces of the specimen during a test. End faces are machined smooth and accurately parallel. Specimens are loaded along one of the longer dimensions of the specimen between parallel platens the faces of which are lubricated with oil.

Extensometers are used to measure changes in the platen separation, and nominal strains are derived from the original specimen length. Some compression results are shown in Figure 2 obtained on a 10 mm square specimen cut from the gauge region of a standard tensile specimen. The results shown are for a specimen loaded along the long axis of the specimen. The results of tests loaded at right angles to this axis can be used to reveal the level of anisotropy in the specimen caused by melt flow into the mould.

Chapter 4

Determination of model parameters

- General
- Tensile modulus and Poisson’s ratio
- Von Mises model parameters
- Linear Drucker-Prager model parameters
- Cavitation model parameters
- Rate-dependent plasticity
- Rate-dependent elasticity

General

In this section, procedures for the analysis of test data are described for determining the parameters in the elastic-plastic models introduced in Chapter 2. The test data presented in Chapter 3 for the rubber-toughened, propylene-ethylene copolymer are used to illustrate typical results from the analyses.

Tensile modulus and Poisson's ratio

These properties are usually used to characterise linear, elastic behaviour and are required for the application of all elastic-plastic models. Values for E and ν^e are usually obtained following the standard tensile test for plastics [2] using specimens having the ISO standard geometry. The test is carried out under constant speed which leads to curvature in stress/strain behaviour even at very low strains, arising from the linear viscoelastic behaviour of the polymer. This is illustrated in Figure 8, which shows the tensile results from Figure 2 plotted over a smaller strain range.

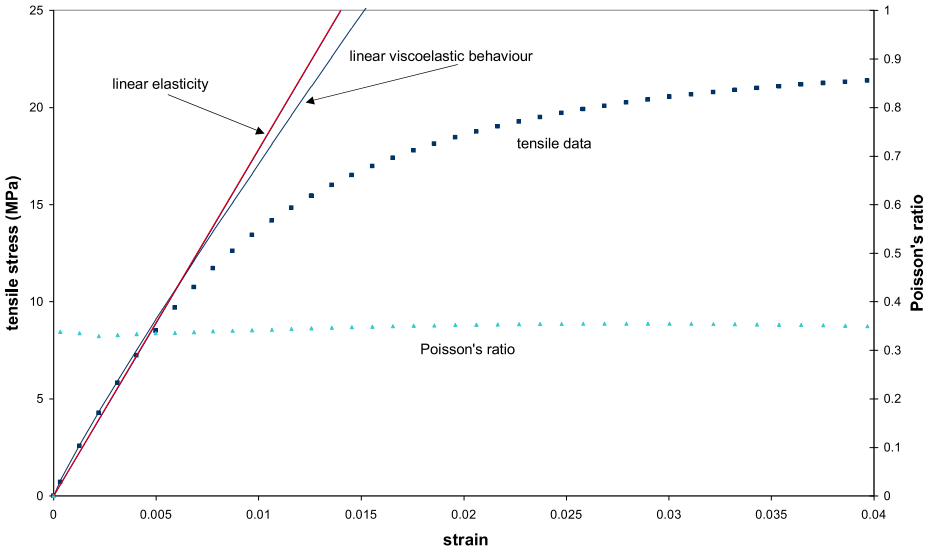

***Figure 8**. Determination of a value for the tensile modulus of a viscoelastic material for elastic-plastic analyses.*

The curvature at small strains makes the determination of a tensile modulus using this test dependent on the strain level selected. The ISO Standard specifies recording the gradient of the secant between strains of 0.0005 and 0.0025. This upper strain limit is too low for elastic-plastic analyses which require a strain limit that identifies the onset of material non-linear

behaviour that is attributed to plastic deformation in elastic-plastic models. The linear fit to the low-strain data in Figure 8 gives a value for tensile modulus of 1.78 GPa and implies a limit for elastic behaviour, and hence and the onset of plasticity, at a strain of 0.004. The value for the elastic component of Poisson's ratio is 0.37. The inability to define the elastic modulus with less ambiguity results from the need to represent viscoelastic behaviour as elastic-plastic.

Associated with viscoelastic behaviour is a dependence of modulus on strain rate. Finite element systems suitable for simulating the impact performance of plastics do not generally take account of rate-dependent elastic behaviour. It is therefore worthwhile determining tensile properties at a strain rate corresponding to some mean value for the range of rates generated in the event to be simulated.

Von Mises model parameters

The property requirements for this model have been introduced earlier in Chapter 2 and are

- Young's modulus E and elastic Poisson's ratio ν^e
- tensile hardening curves $\sigma_T(\varepsilon_T^p)$ over a range of strain rates.

Determination of the hardening curve requires tensile measurements out to large strains, and these are best obtained using the test specimen geometry introduced in Chapter 3 which gave the results shown in Figure 6. Derivation of the hardening function from these data involves subtracting the elastic component of strain at each stress from the total strain to give the plastic component using equation (2). The resulting plot of true stress against true plastic strain is shown in Figure 9. Also shown are plastic Poisson's ratio values. The determination of hardening curves at higher strain rates is described in section on rate-dependent plasticity.

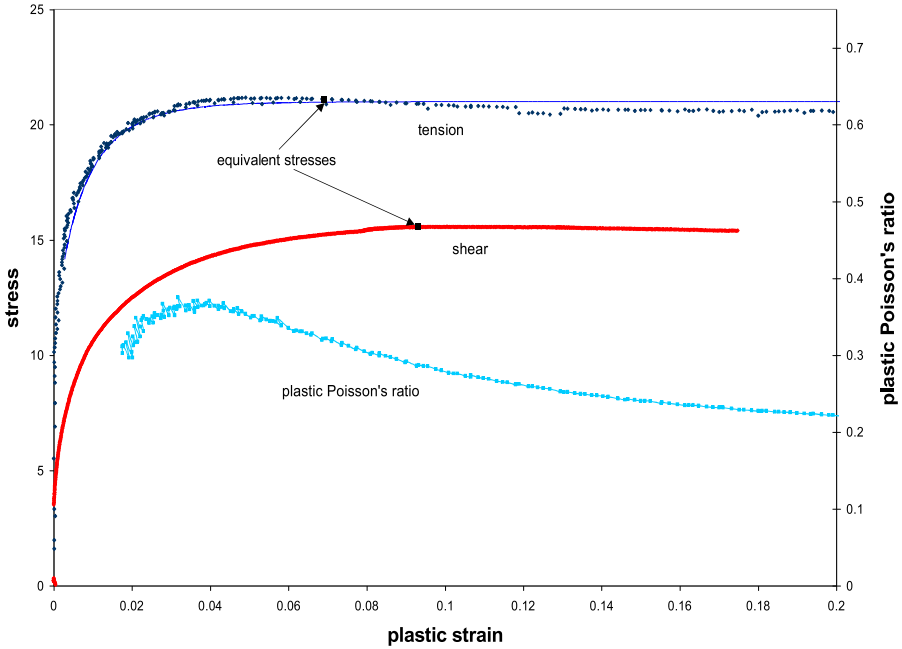

***Figure 9**. Hardening curves in tension and shear and plastic Poisson's ratio. The tensile curve is derived from the data in Figure 6 and the shear curve from Figure 2. The continuous line through the tensile data is based on equation (28).*

Linear Drucker-Prager model parameters

In this section, the results for the propylene-ethylene copolymer are analysed to obtain parameters for the linear Drucker-Prager model, which are shown in Table 1. The property requirements for this model have been introduced in Chapter 2 and are

- Young's modulus E and elastic Poisson's ratio ν^e
- tensile hardening curves $\sigma_T(\varepsilon_T^p)$ over a range of strain rates
- the hydrostatic stress sensitivity parameter μ
- the flow parameter μ'

The first two requirements are identical to those for the von Mises model described above. Determination of the parameter μ requires the measurement of hardening behaviour under an additional stress state. Measurements under shear, although not routine, are probably achievable with greater precision than under uniaxial compression. Experimental shear stress vs shear strain data for the propylene copolymer, obtained using the test method introduced in Chapter 3, are shown in Figure 2. Plastic shear strains $\varepsilon_S{}^p$ corresponding to shear yield stresses σ_S are calculated using the expression

$$\varepsilon_S^p = \varepsilon_S - \frac{\sigma_S}{G} \tag{25}$$

which is analogous to equation (2) with the shear modulus G replacing the tensile modulus. The resulting shear hardening curve $\sigma_S(\varepsilon_S^p)$ is compared with tensile hardening data in Figure 9. Through equation (9), yield stresses σ_T and σ_S on each of the curves in Figure 9 define a yield surface which expands with increasing plastic strain. Points σ_T, ε_T^p, on the tensile curve and σ_S, ε_S^p, on the shear curve lie on the same surface if the plastic work associated with these points is the same. This requirement leads to the relationship between equivalent points on each curve defined in equation (14).

One pair of equivalent points is shown on the curves in Figure 9. These stress values can be used to determine a value for the parameter μ using equation (13) reproduced below.

$$\mu = 3\left[\left(\sqrt{3}\,\sigma_S/\sigma_T\right) - 1\right] \tag{26}$$

For some polymers, the linear Drucker-Prager criterion is a valid description of yielding. The derived value for μ will then be independent of the stress pair used in the derivation. For polymers where cavitation accompanies yielding, the value for μ will depend on the stress pair chosen. This results from the influence of cavitation on tensile behaviour which is absent in the shear results and which gives rise to the different shapes of the tensile and shear hardening curves for these materials as is evident in Figure 9. An apparent, or average, value for μ is recorded in Table 1 obtained from the equivalent stresses shown in Figure 9.

A value for the flow parameter μ' can be derived using equation (18) with a value for the plastic component of Poisson's ν^p from Figure 9. The value for μ' recorded in Table 1 is obtained using a value for $\nu^p = 0.22$ in Figure 9 at a plastic strain of 0.2. As with the determination of μ, the derived value for μ' depends on which value of ν^p is chosen for the calculation. This once again demonstrates that the Drucker-Prager model cannot accurately predict the deformation behaviour of certain types of polymer.

Parameter	Value
E (GPa)	1.78
ν^e	0.37
$\sigma_T(\varepsilon_T^p)$ (MPa)	Fig. 9
μ	0.84
μ'	0.69

Table 1. *Values for the toughened propylene copolymer parameters in the linear Drucker-Prager model at a strain rate of 0.01 s^{-1}.*

Some of the limitations in using the linear Drucker-Prager model to describe the non-linear behaviour of the propylene-ethylene copolymer are illustrated by comparisons of measured and predicted curves of shear and compressive stresses and Poisson's ratio with strain shown in Figure 10. The predictions were obtained using the properties and parameters in Table 1.

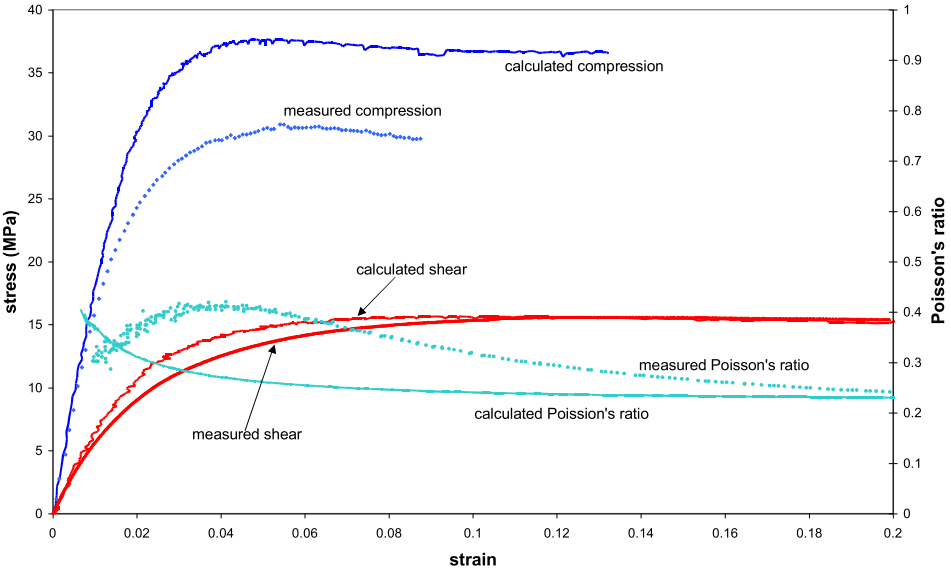

Figure 10. *Comparison of measured and predicted deformation behaviour using the linear Drucker-Prager model and the parameters in Table 1. Plastic-strain hardening behaviour is defined by tensile data in Figure 9.*

Cavitation model parameters

The inability of the linear Drucker-Prager model to describe both shear and compressive behaviour and the nature of the fall in Poisson's ratio with strain arises because the model does not take account of the nucleation of numerous small cavities on the yield behaviour under stress states where there is a significant hydrostatic component. These cavities nucleate over a range of tensile strain, and this gives rise to the different shape of the tensile curve compared with either the shear or compressive curve as seen in Figure 10 where the tensile hardening curve is used to predict shear and compressive behaviour. The NPL developed cavitation model attempts to include the influence of cavitation on deformation behaviour through adaption of the yield criterion and the introduction of a cavity nucleation criterion that relates the volume fraction of nucleated cavities to the magnitude of the volumetric strain.

Due to the increased complexity of the material model, significantly more material parameters are required to describe the material behaviour. These necessitate a larger programme of experimental tests to be conducted including tension, shear and compression testing. A full overview of the model and parameter calculation is given in [6, 7]. The required parameters are outlined below

- Young's modulus E and elastic Poisson's ratio ν^e
- effective shear hardening curves $\sigma_o(\varepsilon_o^p)$ over a range of strain rates, Figure 11. These replace tensile hardening curves in the previous models.
- a hydrostatic stress sensitivity parameter μ calculated from measurements of yield stress under shear and compression at equivalent yield points on the curves (analogous to equation (14) and Figure 9 for linear Drucker-Prager calculation).
- the volume fraction of cavities v_C in the fully cavitated material plus parameters ε_{1V}, ε_{2V} and β that relate the volume fraction of nucleated cavities f to the volumetric strain produced by the applied stress. These parameters are obtained by an iterative process to achieve satisfactory predictions of the shape of the tensile stress-strain curve in the strain range associated with cavity nucleation, Figure 12.
- a cavity interaction parameter q_1 plus parameters σ_{MC} and k in equation (22) that describes how the effective shear yield stress σ_o varies with the volume fraction of the phase in which cavities can form. Studies suggested that the magnitude of these parameters are essentially independent of material types and typical values could be used [11, 12, 14].
- the flow parameter μ'. This influences the decrease in Poisson's ratio with strain seen in Figure 6. A value of μ' can be derived using the cavitation model to obtain satisfactory fits to the Poisson's ratio data.

For the cavitation model, hardening behaviour is expressed by a curve of the effective stress σ_o against the effective plastic strain ε_o^p . These quantities are obtained from shear stress (σ_S) and shear strain (ε_S) data in Figure 2 using the relationships

$$\sigma_o = \sqrt{3}\sigma_S \text{ and } \varepsilon_o^p = \varepsilon_S^p/\sqrt{3} \tag{27}$$

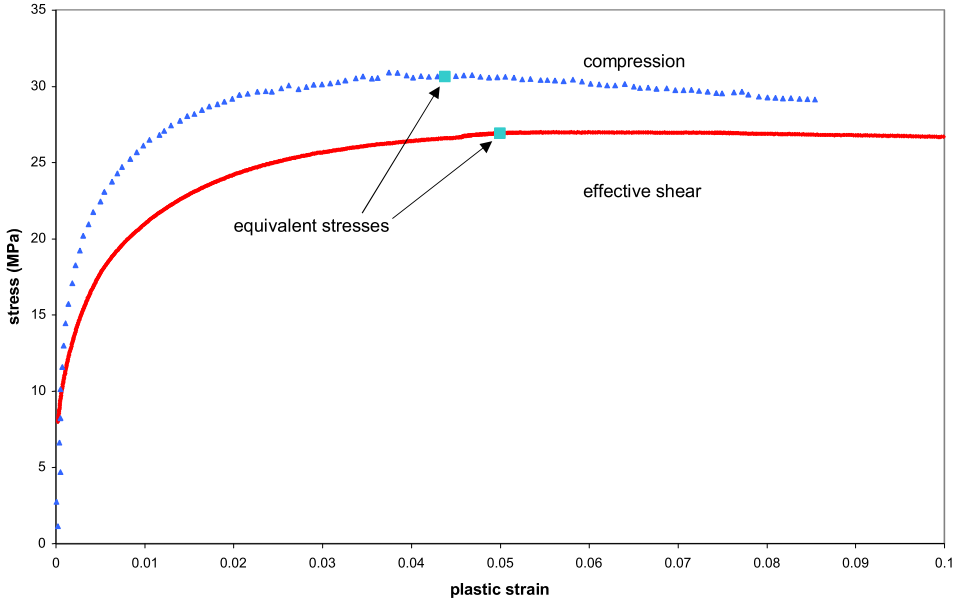

Figure 11. *Hardening curves under compression $\sigma_C\left(\varepsilon_C^p\right)$ and shear $\sigma_0\left(\varepsilon_0^p\right)$ derived from the results in Figure 2. A pair of equivalent stresses is shown for the calculation of the parameter μ in the cavitation model.*

It is apparent how much additional effort is required to obtain material parameters for more complex models. A set of parameters for the propylene-ethylene copolymer is given in Table 2.

Parameter	Value
E (GPa)	1.78
ν^e	0.37
$\sigma_o(\varepsilon_o^p)$ (MPa)	Fig 11
μ	0.36
v_C	0.40
k	2.5
q_1	1.5
$\mu_1^{'}$	0.13
ε_{1v}	0.003
ε_{2v}	0.01
β	0.9

Table 2. *Toughened propylene copolymer parameters in the cavitation model at a strain rate of 0.01 s^{-1}.*

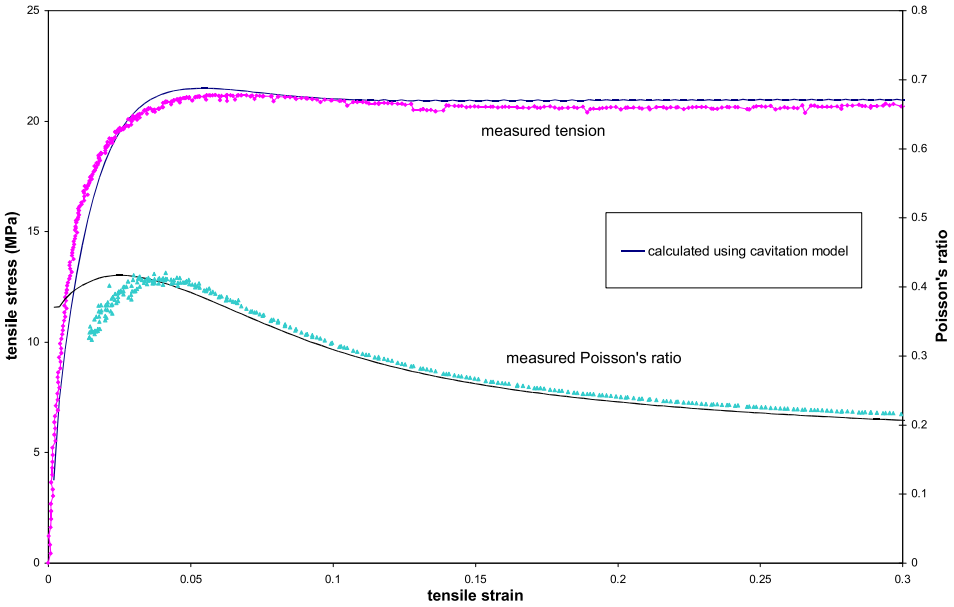

Figure 12. *Comparison of measured tensile behaviour with predicted curves using the cavitation model with the parameters in Table 2.*

Rate-dependent plasticity

General

Whichever model is used for a stress analysis, more accurate predictions will be made if the dependence of properties on strain rate is taken into consideration. In many finite element systems, facilities are available for including the dependence of yield behaviour on strain rate (rate-dependent plasticity). There are problems with the measurement of properties at impact strain rates ($\cong$ 1000 s^{-1}) arising from the effects of resonances in the specimen and test assembly. A method is described in this section for the determination of properties at high strain rates by modelling behaviour at low and moderate rates and calculating high rate behaviour by extrapolation.

The rate dependence of low-strain (linear viscoelastic) behaviour is in general not included in elastic-plastic models, but brief reference is made in the next section showing how the rate-dependence of a stress/strain curve can be related to stress relaxation results.

Tensile behaviour

The characterisation of plastic behaviour for elastic-plastic models requires determination of a hardening function $\sigma(\varepsilon^p)$, which is most conveniently measured in tension. For an analysis with rate-dependent plasticity, it is necessary to determine the variation in the hardening curve with strain rate. A procedure is now described for determining properties by

- modelling the shape of experimental hardening curves at low and moderate strain rates
- determining the variation of model parameters with strain rate
- deriving hardening behaviour at high strain rates by extrapolation

Stress/strain curves measured in tension over a range of test speeds ranging from 0.01 mm/s to 100 mm/s are shown in Figure 13. These were obtained on waisted specimens of the geometry shown in Figure 4 cut from the central region of injection moulded standard tensile specimens.

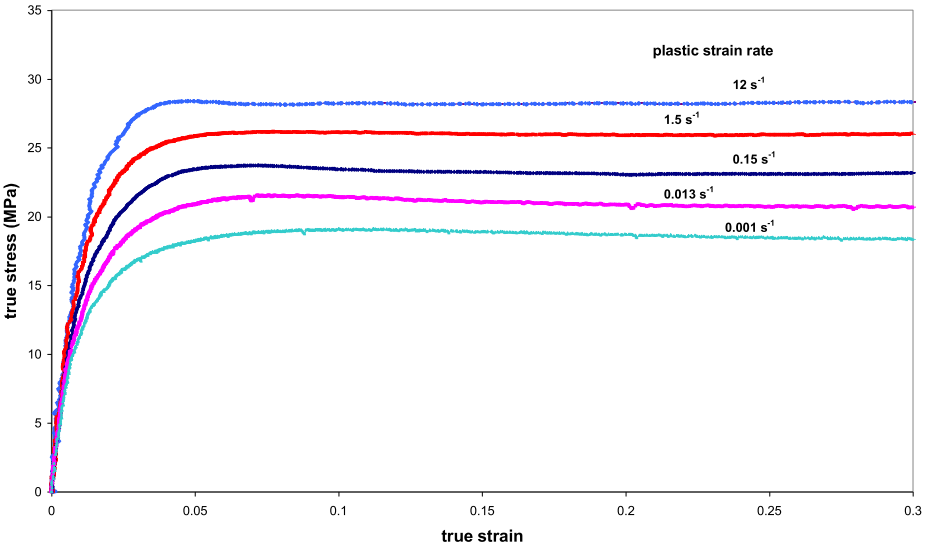

Figure 13. *Tensile stress/strain curves measured on waisted specimens at test speeds ranging from 0.01 mm/s to 100 mm/s.*

Hardening curves $\sigma_T(\varepsilon_T^p)$ derived from these data are shown in Figure 14. These curves have been fitted using the function

$$\sigma_T(\varepsilon_T^p) = \sigma_i + (\sigma_f - \sigma_i)\left(1 - \exp - (\varepsilon_T^p/\varepsilon_a)^n\right) \quad (28)$$

Where σ_i is the stress at zero plastic strain, σ_f is the limiting stress at high plastic strains and ε_a and n are parameters that determine the mean strain and the strain range over which the increase of σ_T with ε_T^p occurs. Values for the parameters used to obtain the fits in Figure 14 are shown in Table 3.

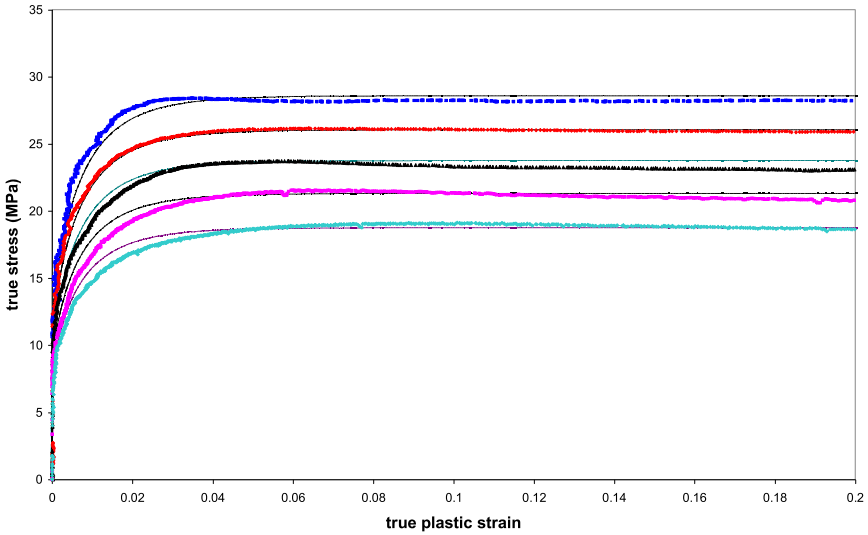

***Figure 14**. Hardening curves derived from the results in Figure 13 and modelled using equation (28) and the parameters in Table 3.*

Plastic strain rate (s^{-1})	σ_f (MPa)	σ_i	ε_a	n
12	28.6	11.5	0.007	0.8
1.5	26.1	10.5	0.007	0.8
0.15	23.6	9.5	0.007	0.8
0.013	21.3	8.5	0.007	0.8
0.001	18.8	7.5	0.007	0.8

***Table 3.** Values for the parameters in equation (28) used to obtain the fits to tensile data in Figure 14.*

The calculated curves were obtained with a constant value for ε_a and n and an approximately constant ratio of σ_i/σ_f = 0.4. Although these fits are adequate, it is evident that the peak stress is reached at lower plastic strains as the strain rate increases, implying that ε_a is decreasing with strain rate. Better fits can, accordingly, be obtained with the parameters given in Table 4 as shown in Figure 15.

Plastic strain rate (s^{-1})	σ_f (MPa)	σ_i	ε_a	n
12	28.6	11.5	0.006	0.8
1.5	26.1	10.5	0.007	0.8
0.15	23.6	9.5	0.008	0.8
0.013	21.3	8.5	0.009	0.8
0.001	18.8	7.5	0.01	0.8

Table 4. *Repeat of Table 3 but with values for ε_a decreasing with strain rate to give better fits to experimental data.*

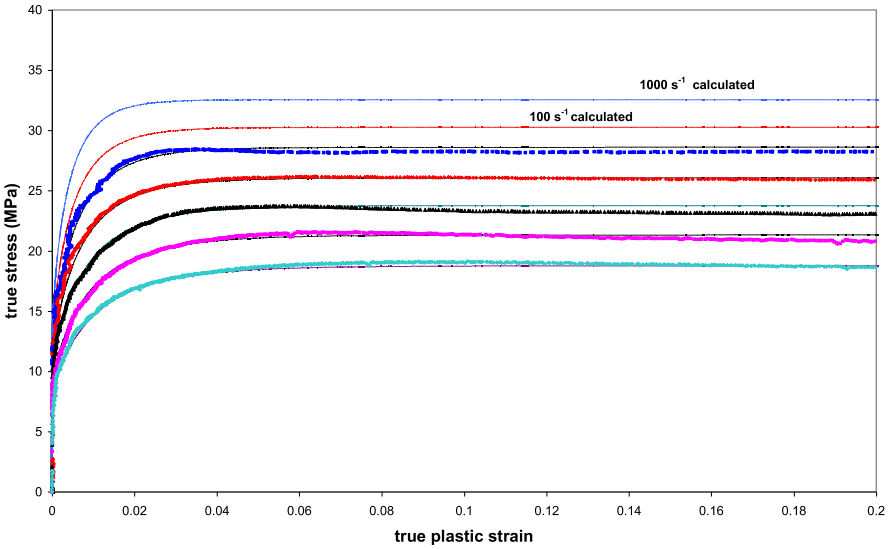

Figure 15*. Hardening curves from Figure 14 modelled using the alternative set of parameters in Table 4. Curves at higher rates calculated using parameters from Figure 16 with equation (29).*

The increase in σ_f with plastic strain rate can be described by the Eyring function.

$$\sigma_f = \sigma_{fo} + A \log \dot{\varepsilon}_T^p \tag{29}$$

Where σ_{fo} and A are material parameters. This is demonstrated in Figure 16 which gives values for σ_{fo} = 25.8 MPa and A = 2.4 MPa when strain rate is in units of s^{-1}. The variation of ε_a can be described by a similar function

$$\varepsilon_a = \varepsilon_{ao} - B \log \dot{\varepsilon}_T^p \tag{30}$$

With ε_{ao} = 0.007 and B = 0.001.

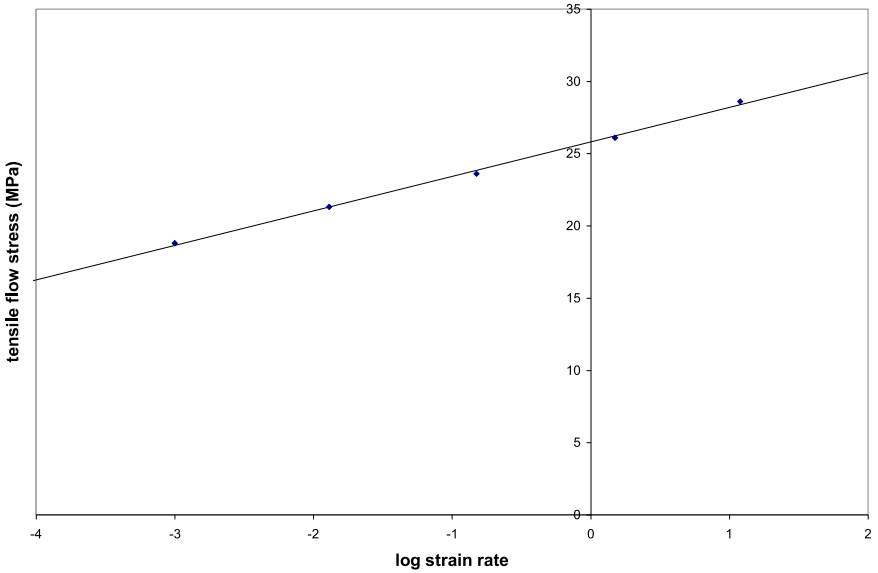

Figure 16. *Plot of flow stresses σ_f from Tables 3 and 4 against log plastic strain rate.*

Equations (28), (29) and (30) together with a knowledge of 6 material parameters (σ_{fo}, A, σ_i/σ_f, ε_{ao}, B and n) can therefore be used to derive tensile hardening curves at any arbitrary strain rate. This information constitutes the hardening properties required by an analysis with rate dependent plasticity using the von Mises or linear Drucker-Prager models. The cavitation model requires hardening properties in the form of effective shear data (see the next section). If a lower accuracy in describing the shape of hardening curves at strains below 0.04 is acceptable, then the number of parameters reduces to 5 (σ_{fo}, A, σ_i/σ_f, ε_{ao} and n). Curves at

high strain rates associated with impact speeds calculated using the parameters listed in Table 4 are shown in Figure 15. The precision of these data depends upon the validity of the extrapolation using equation (29) beyond the range of measured values in Figure 16 and is a subject for further study.

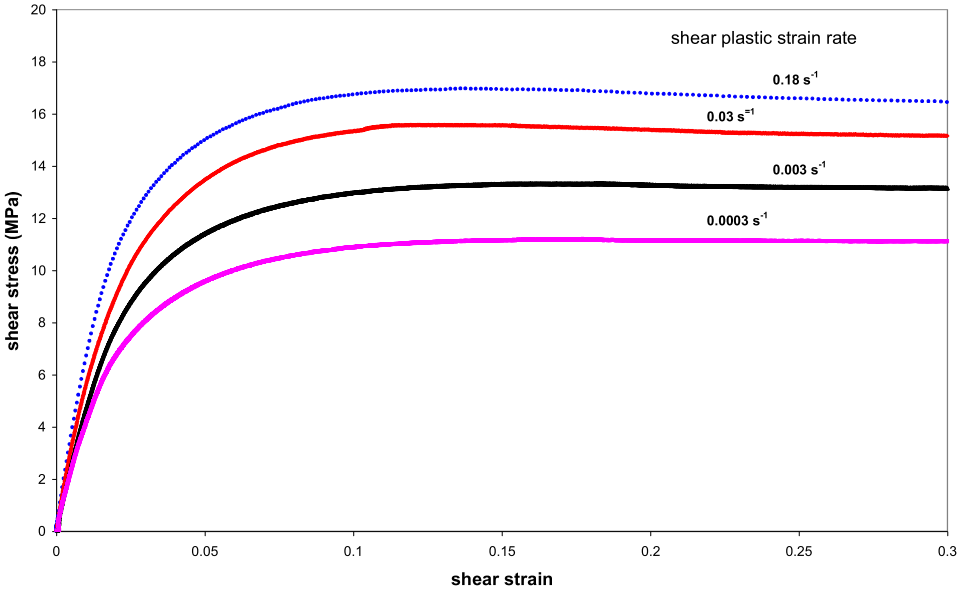

Figure 17. *Shear stress/strain curves measured at the strain rates shown.*

Shear behaviour

Plastic strain hardening in the cavitation model is defined by hardening curves determined under a shear stress. Stress/strain curves measured using the shear test in Chapter 3 at different strain rates are shown in Figure 17. Hardening behaviour is expressed by a curve of the effective stress σ_o against the effective plastic strain ε_o^p . Hardening curves for the effective stress have been derived from the data in Figure 17 and are shown in Figure 18.

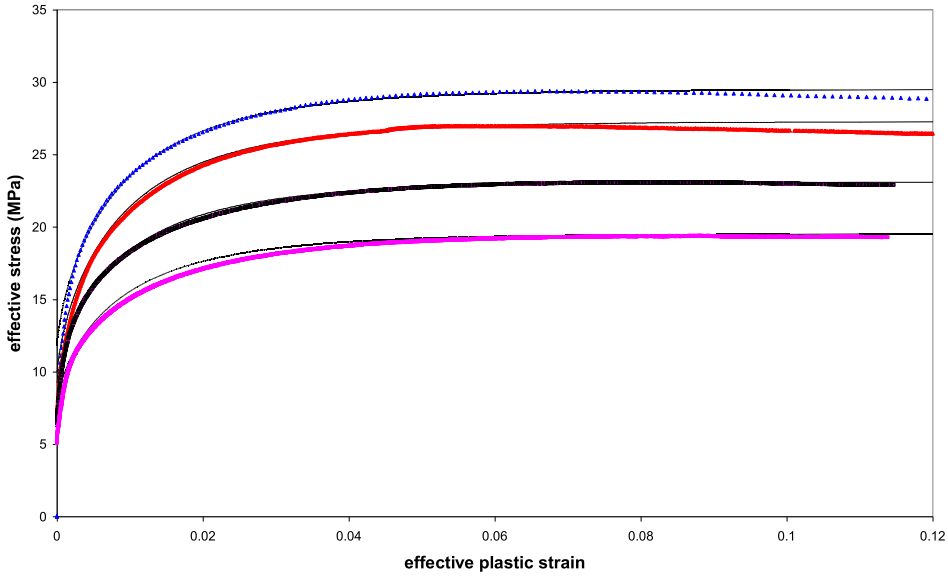

***Figure 18**. Shear hardening curves derived from the results in Figure 17 and modelled using equation (31) with the parameters in Table 5.*

The curves in Figure 18 have been modelled using the same function equation (28) that was used to model tensile behaviour

$$\sigma_o(\varepsilon_o^p) = \sigma_{oi} + (\sigma_{of} - \sigma_{oi})\left(1 - \exp - (\varepsilon_o^p/\varepsilon_{oa})^{n_o}\right) \qquad (31)$$

Where σ_{oi} is the effective shear stress at zero plastic strain, σ_{of} is the limiting stress at high plastic strains and ε_{oa} and n_o are parameters that determine the mean strain and the strain range over which the increase of σ_o with ε_o^p occurs. Values for the parameters in equation (31) are shown in Table 5.

Effective shear plastic strain rate $\dot{\varepsilon}_o^p$ (s^{-1})	σ_{of} (MPa)	σ_{oi} (MPa)	ε_{oa}	n_o
0.1	29.5	11.5	0.009	0.75
0.017	27.3	10	0.009	0.75
0.0017	23.1	9.5	0.009	0.75
0.00017	19.5	7.5	0.009	0.75

Table 5. *Values for the parameters in equation (31) used to fit the shear data in Figure 18.*

Constant values for the parameter ε_{oa} in Table 5 show that, in contrast to tensile results, the hardening curve shape remains constant with strain rate and simply shifts up the stress axis with increasing rate. It can be seen from the results in Table 5 that the ratio σ_{oi}/σ_{of} may again be assumed constant at a value of 0.4. Values for σ_{of} from Table 5 are plotted against log effective shear plastic strain rate in Figure 19 and are compared with tensile data from Figure 16. The variation of σ_{of} with log strain rate $\dot{\varepsilon}_o^p$ is again accurately linear and can be represented by the Eyring equation

$$\sigma_{of} = \sigma_{ofo} + C \log \dot{\varepsilon}_o^p \qquad (32)$$

where, from Figure 19, σ_{ofo} = 33.1 MPa and C = 3.6.

The results in Figure 19 show that the ratio of tensile and effective shear stresses when cavitation is complete varies with strain rate. The probable reason for this is that the cavity volume fraction when cavity nucleation is complete increases with strain rate. This conclusion is supported by measurements of Poisson's ratio at very low test speeds. These results show a smaller drop in value than is observed in results at higher speeds (Figure 6) which is consistent with a lower value for v_C. As the strain rate is lowered, the shear yield stress decreases thereby promoting shear yielding in favour of cavitation in certain regions of the polymer. At higher rates, cavitation takes place in these regions, but there will presumably be a limit to the increase in v_C with strain rate when cavities have formed in all the available regions in the polymer. This means that, at higher strain rates, the gradient of the tensile line should increase thereby introducing some uncertainty in the linear extrapolation of equation (29).

Extrapolation of shear data using equation (32) does not suffer from this restriction since the gradient is not influenced by the magnitude of v_C. However, when determining a value for the parameter v_C for use in the cavitation model, experimental data should be used that has been measured at as high a strain rate as feasible in order to derive a value for v_C appropriate to impact strain rates.

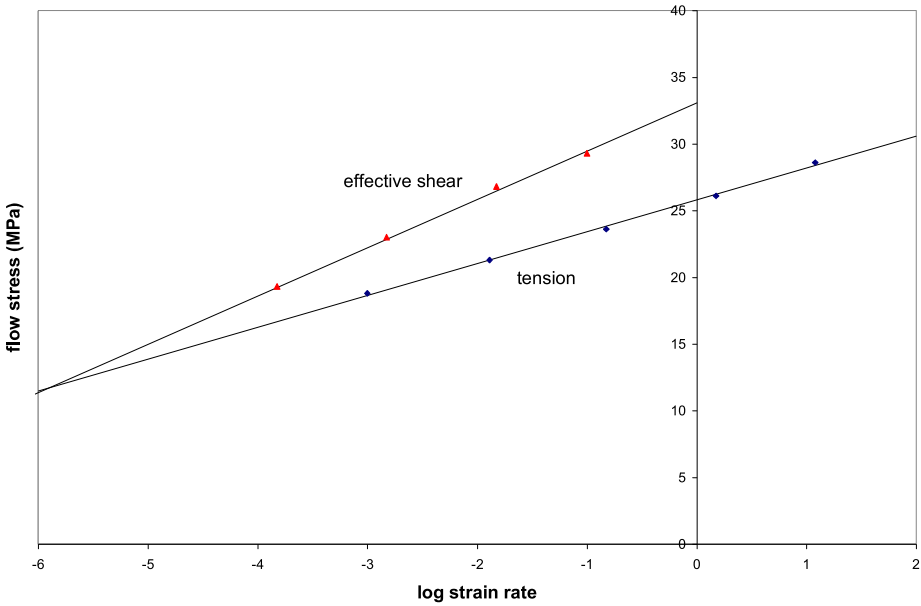

Figure 19. *Comparison of plots of tensile and effective shear flow stresses against log strain rate.*

Rate-dependent elasticity

Stress/strain curves in constant strain rate tests on viscoelastic materials are not straight lines even at low strains where behaviour is linear. This arises because properties depend upon time under load which is changing throughout the test. The ISO standard for tensile testing specifies the determination of a tensile (secant) modulus which is the gradient of the line joining points on the curve at strains of 0.0005 and 0.0025. This gradient changes with the strain rate and hence speed of the test. This is not a rigorous characterisation of low-strain behaviour but is satisfactory for glassy polymers that are only slightly viscoelastic. Where greater precision is required, the shape of a stress/strain curve over the range of strains where behaviour is linear viscoelastic can be related to results from a single stress relaxation test.

A stress relaxation function under tension E(t) relates the time varying stress $\sigma(t)$ to the tensile strain ε under a situation where the strain is held constant with time. So

$$\sigma(t) = E(t)\varepsilon \tag{33}$$

A tensile test under a constant strain rate can be considered as a series of step increases in strain with strain increment $\Delta\varepsilon$ for periods Δt. For strain levels where behaviour is linear, the stress response to the step loading can be derived by superposition as follows

$$\sigma(t) = E(t)\Delta\varepsilon + E(t-\Delta t)\Delta\varepsilon + E(t-2\Delta t)\Delta\varepsilon + \ldots \quad (34)$$

The situation where the strain is applied smoothly at constant velocity can be realised by letting $\Delta\varepsilon \rightarrow 0$ in which case equation (34) reduces to the integral equation

where s is a dummy time variable.

By defining a new time variable u = (t - s) and noting that $d\varepsilon/ds = \dot{\varepsilon}$, equation (35) becomes

$$\sigma(t) = \int_0^t E(t-s)\frac{d\varepsilon}{ds}ds \quad (35)$$

$$\sigma(t) = \dot{\varepsilon}\int_0^t E(u)du \quad (36)$$

Stress relaxation data for the propylene copolymer studied in this Guide are shown in Figure 20 and have been modelled with satisfactory accuracy by the function

$$E(u) = E_R + Du^{-n} \quad (37)$$

where E_R = 820 MPa, D = 740 MPa.s^n and n = 0.17.

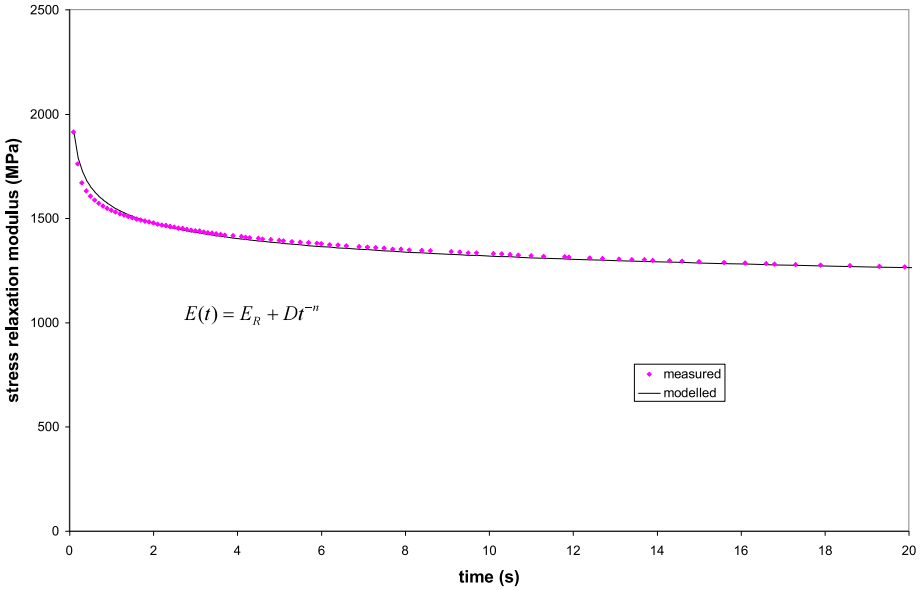

Figure 20. *Stress relaxation data modelled using equation (37).*

Inserting equation (37) into (36) and noting that $\dot{\varepsilon} = \varepsilon/t$ gives the equation of a stress/strain curve under constant strain rate as

$$\sigma(\varepsilon) = E_R\varepsilon + \frac{D\dot{\varepsilon}^n\varepsilon^{1-n}}{1-n} \qquad (38)$$

Equation (38) captures the non-linear variation of stress with strain and the dependence on strain rate. Predicted curves at selected strain rates are shown in Figure 21 and are compared with experimental data at a strain rate of 0.01 s^{-1}. The departure of predicted and measured values at strains above 0.005 implies that this strain level marks the limit of linear viscoelastic behaviour. It should be noted that values for the parameters in the stress relaxation function, equation (37), were obtained by comparison with experiment at times > 1s. The applicability of these values at times << 1s is not known so the accuracy of predicted stress/strain behaviour in Figure 21 at high strain rates is uncertain.

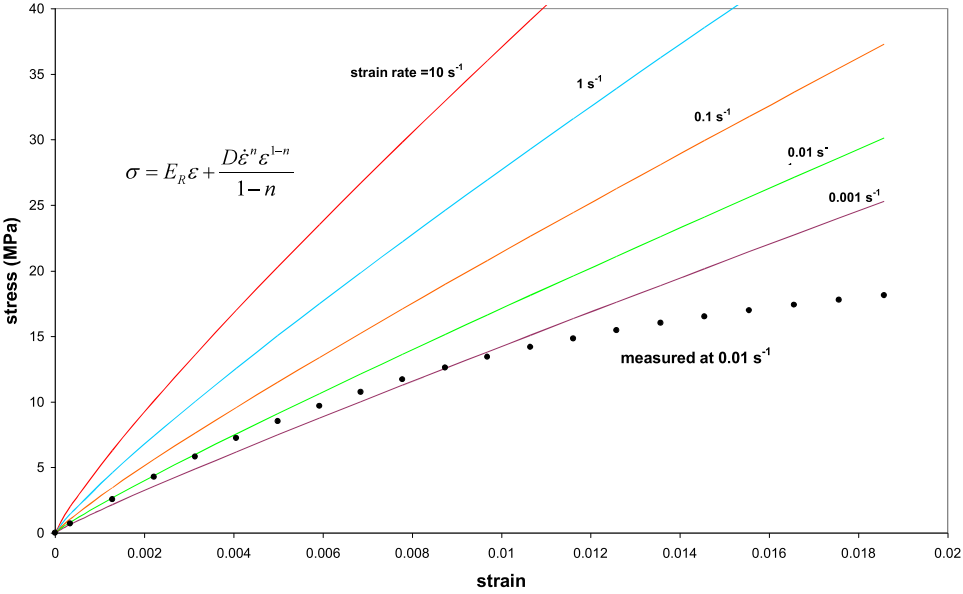

Figure 21. *Stress/strain curves at different strain rates calculated using equation (38) and compared with measured values at 0.01 s^{-1}.*

Chapter 5

Application of Finite Element Analysis

- FEA Introduction and basics
- Materials models
- Predicting performance

FEA introduction and basics

A finite element system can be used to calculate the forces, displacements, stresses and strains throughout the components involved in an impact situation. An array of 2- or 3-dimensional elements is used to define the shape and size of the components. The elastic-plastic models that are needed to describe the deformation behaviour of plastics materials have been described in the previous sections, along with details on the measurement and calculation of model parameters.

This chapter covers some of the main factors that need to be considered when generating a finite element analysis. When appropriate, examples demonstrating these factors are given. The examples will be used to illustrate the application of FE methods for predicting the deformation of car components. All analyses use parameter values obtained for the toughened propylene copolymer presented in Tables 1 and 2 in Chapter 4. The two components analysed were subcomponents cut from the interior door panel of a Land Rover vehicle. The locations of the subcomponents within the moulding are shown in Figure 22. The armrest subcomponent (labelled b in Figure 22) is part of the armrest region. The region labelled a in Figure 22 is a curved area cut from the upper boundary of the panel and is stiffened by ribs. This part was referred to as the toptrim.

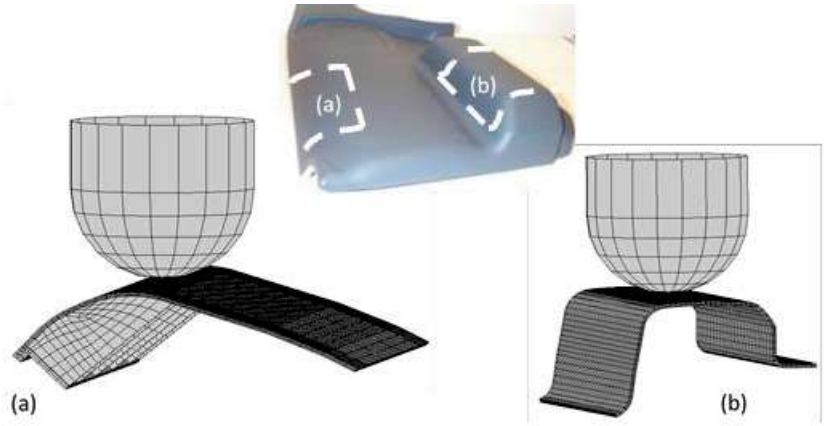

Figure 22. *Finite element meshes used for (a) toptrim and (b) armrest components.*

Clamping devices were manufactured in-house to support some of the boundaries of each subcomponent specimen under conditions that can be simulated in the FE analyses. The subcomponent specimens were loaded in a universal testing machine by a hemispherical surface of diameter 80 mm acting on the centre of the exposed surface of each subcomponent

as shown in Figures 22a and 22b. Measurements were made of the force applied by the hemisphere and the displacement of the hemisphere into the surface of the subcomponent. These experimental data have been used to illustrate the ability of finite element analysis to predict deformation behaviour under impact loading.

Element type

An element mesh is used to represent the component geometry. The geometry needs to be modelled as accurately as possible, taking account of any symmetry, which would reduce the size of the model. A pre-processor such as Abaqus /CAE [5] is used to generate the geometry. Once this geometry has been created, an FE mesh can be applied to it. There are several factors to consider when meshing a geometry, such as element type, mesh density etc. The choice of elements can greatly influence results obtained from an analysis. In some cases the difference in results between element types may not be visible in force/extension plots, but maybe observed in the values obtained for stress or strain contours. There is a wide range of element families available in FE packages such as Abaqus [5], ranging from simple beam elements to solid (continuum) elements. There are also a variety of elements within each element family, each with their own advantages and disadvantages.

Elements used in impact analysis are likely to be either solid (continuum) or shell elements, depending on the size of the component to be modelled. These are suitable for linear analysis and also for complex nonlinear analyses involving plasticity and large deformations. Stress/displacement elements are used in the modelling of linear or complex nonlinear mechanical analyses that possibly involve contact, plasticity and/or large deformations. All the stress/displacement elements in Abaqus are based on the Lagrangian or material description of behaviour, where the element deforms with the material.

There are a number of continuum elements available within the FE element libraries. The elements selected need to be appropriate for each particular analysis. Quadrilateral elements and hexahedra have a better convergence rate than triangular and tetrahedral elements. First-order quadrilateral elements perform best if their initial shape is approximately rectangular with a maximum aspect ratio of 7:1. The elements become much less accurate when they are initially distorted. When modelling high loading rates, the first order form of continuum elements is recommended. Second order elements are also available and these provide higher accuracy than first order elements for ‘smooth’ problems that do not involve complex contact conditions of impact. Second order elements have more nodes per element than first order elements i.e. have a midside node. First and second order elements should not

be mixed within a mesh without applying constraints, otherwise problems can be caused due to the different types of interpolation used within the two element types. The chosen FE solver controls some element selections; for instance, in Abaqus/Explicit the only quadrilateral or hexahedral continuum elements available are reduced-integration first-order elements.

For structural applications, the FE element libraries for two-dimensional continuum elements include plane stress, plane strain and generalised plane strain elements. Plane stress elements can be used when the out-of-plane dimension of a body is small relative to its in-plane dimensions. The plane stress element assumes that the out-of-plane stress is zero. Modelling with this element generally applies to thin, flat bodies. In contrast, plane strain elements are generally used for modelling bodies where the out-of-plane dimension is much larger than the in-plane dimensions. In these elements it is assumed that the out-of-plane strains are zero. An alternative form of plane strain element is the generalised plane strain element. In this case the formulation used places the model between two rigid planes that can only move closer or further apart. It is assumed that the deformation of the model is independent of the axial position so the relative motion of the two planes causes a direct strain in the axial direction only. There are no transverse shear strains. Three dimensional continuum elements avoid the artificial distinction between plane stress and plane strain. These elements are used to model more complex three-dimensional structures. However, 3D elements normally lead to larger computational problems and hence, longer run times.

Shell elements are used to model structures in which one dimension, the thickness, is significantly smaller than the other dimensions. Conventional shell elements use this condition to discretize a body by defining the geometry at a reference surface. Conventional shell elements have displacement and rotational degrees of freedom. The shell's nodes and normal definitions define the reference surface for conventional shell elements. The reference surface is typically coincident with the shell's midsurface. However, it is sometimes more convenient to define the reference surface as offset from the shell's midsurface. For example, CAD surfaces usually represent either the top or bottom surface of the shell. In this case it may be easier to define the reference surface to be coincident with the CAD surface and, therefore, offset from the shell's midsurface. Shell offsets can also be used to define a more precise surface geometry for contact problems where shell thickness is important. Shell elements are computationally less expensive than solid elements, leading to faster analysis run times.

EXAMPLE: Comparison of solid and shell elements

In this example predictions obtained from different element types are compared. The toptrim subcomponent of the car interior door trim (see Figure 22) was meshed twice, with solid (continuum) and shell elements respectively. The toptrim subcomponent is a thin (approximately 2 mm thick) curved surface, with strengthening ribs on the underside. In both analyses, a hemispherical indenter impacted the subcomponent at a rate of 10 mm/s. The force-displacement predictions, obtained using the linear Drucker-Prager model detailed in Chapters 2 and 4 and input data from Table 1, have been compared with experimental data in Figure 23. With careful use of the reference surface facility described above, the shell elements can represent the deformation behaviour of the subcomponent as successfully as the solid elements.

Predicted maximum principal stress and strain values have been studied for both analyses, with values being obtained at the peak load, from the region of the mesh where the indenter contacts the toptrim component. The predicted values are presented in Table 6. The stress values are comparable for both element types, but the strains predicted when using shell elements are less than half those predicted from the solid elements.

In this analysis, the hemispherical indenter was modelled as an analytical rigid surface. An analytical rigid surface is a geometric surface with a profile that can be described with straight and curved line segments. This profile can be swept along a generator vector or rotated about an axis to form a three-dimensional surface. An analytical rigid surface is associated with a rigid body reference node, whose motion governs the motion of the surface. This is a useful way of representing an object that is very hard compared to the component being tested and will therefore not deform.

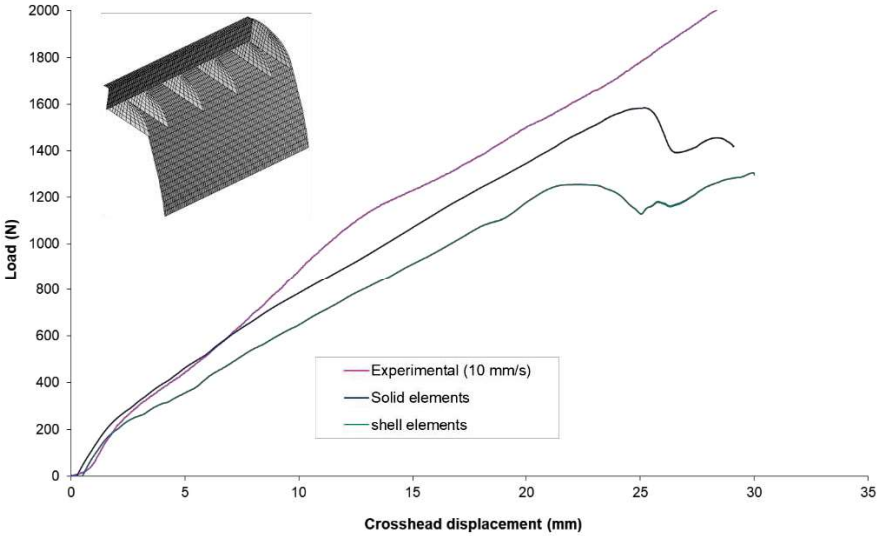

Figure 23. *Comparison of predictions obtained from analyses using solid and shell elements with the measured force-displacement obtained from the toptrim subcomponent.*

Element type	Maximum principal stress (MPa)	Maximum principal true strain
Shell elements	18.3	0.02
Solid elements	21.6	0.07

Table 6. *Maximum Principal Stress and Strain predicted by the linear Drucker-Prager model for the shell and solid element cases at the peak load (toptrim component).*

Mesh density

Mesh density is the number (and therefore size) of elements used within the mesh. It is general practice to run an initial analysis with a coarse mesh. Within the post-processor the deformed shape obtained should be checked to verify that the boundary conditions and loads are behaving as expected. From this analysis, force/extension data can be obtained and checked to make sure that they are physically reasonable. If this is the only required output, then it is not necessary to refine the mesh any further as this should not alter the force/extension behaviour of the model. But if localised stress or strain predictions are required, then further mesh refinement is necessary. Mesh density can affect the strain (and

stress) predictions in regions of strain (or stress) concentration. A smaller element size will generally give a higher maximum value although, at very small element sizes, further dimension changes should cause little effect (mesh convergence).

It is unnecessary to refine the whole mesh if there is only interest in quantitative predictions from areas of strain (or stress) concentration, and a highly refined mesh with high element density would lead to long analysis process times. With the coarse mesh, once satisfied that the model is physically reasonable, contours of stress and strain can be plotted. These contours will highlight any areas of high strain that may require mesh refinement. The size of elements in this area should be reduced until a stable maximum value of stress and strain is achieved i.e. mesh convergence. Ideally, the peak stress or strain contour should be larger than the dimension of a single element. In previous work it was found that, if too small an area of mesh is refined, strain localisations became 'trapped' within the refined mesh. Therefore, a reasonable area needs to be refined with gradually increasing element size out to a coarse mesh in areas where stress and strain values are relatively low and uniform. Once the mesh has been refined satisfactorily and the analysis run, the post-processor should be used to check the continuity of stress contours. With averaged stresses plotted, the contours will look smooth. Unaveraged stresses should also be plotted (quilt plot in Abaqus). If very discontinuous contours are observed, the mesh is no good for stress localisation investigations (although it would be suitable for obtaining force/displacements). When the mesh has been refined enough, even the unaveraged contours appear relatively smooth.

Contact surfaces and boundary conditions

Contact surfaces and boundary conditions can be applied to the geometry of the component to be modelled or to the mesh itself. If the component is likely to be remeshed (for instance when changing mesh density, or altering component dimensions), then it is useful to apply constraints to the geometry, as this will then automatically apply to the new mesh.

Boundary conditions should be applied such that they represent the physical constraints of the modelled component as closely as possible. Constraints can be applied to the three displacement degrees of freedom and the three rotational degrees of freedom. Boundary conditions can also be used to set up symmetry conditions. Where possible, any symmetry in the component should be used to decrease the size of the geometry modelled as this in turn reduces the computational cost of the analysis.

In impact analyses, contact surfaces will need to be included. Contact surfaces are usually defined in pairs. The more deformable of the two surfaces is the secondary surface, while the more rigid surface is the main surface. In the case of a hemispherical indenter impacting an interior door trim component, the top surface of the door trim component would be defined as the secondary surface, while the outer surface of the indenter would be the main surface. In this particular analysis, the indenter was modelled as an analytical rigid surface. Using analytical rigid surfaces instead of defining element-based rigid surfaces provides two important advantages in contact modelling. Many curved geometries can be modelled exactly with analytical rigid surfaces because of the ability to parameterise the surface with curved line segments. The result is a smoother surface description, which can reduce contact noise and provide a better approximation to the physical contact constraint. Using analytical rigid surfaces instead of rigid surfaces formed by element faces may result in decreased computational cost incurred by the contact algorithm.

Friction

When modelling contact, it is also important to consider that friction could be significant between the surfaces in contact. When surfaces are in contact they usually transmit shear as well as normal forces across their interface. The relationship between these two force components is referred to as friction. In Abaqus, the default assumption is that the interaction between two surfaces is frictionless. Friction can be specified between two surfaces by defining friction properties as part of the contact property definition. There is a selection of friction models available within Abaqus [5].

EXAMPLE: Friction versus frictionless surface definitions

Impact analyses of both the toptrim and armrest components, cut from car interior door trim panels (see Figure 22) have been run using the linear Drucker-Prager model (detailed in Chapters 2 and 4, using parameters from Table 1). In both cases a hemispherical rigid indenter impacted the components. When the toptrim component analysis is run without friction, the deforming component stays upright and there is little movement of the indenter over the surface. The inclusion of friction (friction coefficient = 0.2) in this analysis makes very little difference to the predictions, see Figure 24.

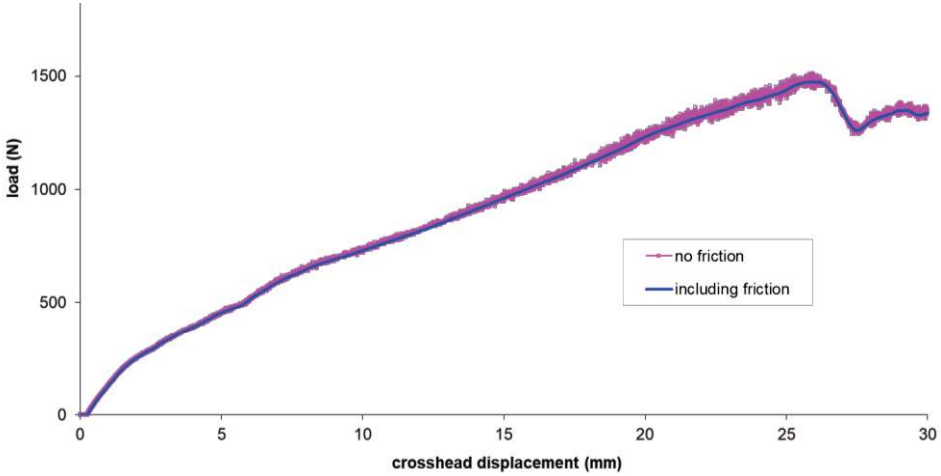

Figure 24. *Comparison of toptrim predicted force-displacement plots run with friction (friction coefficient of 0.2 used) and without friction.*

With the armrest component, an FE analysis run without friction predicts that the component collapses to one side, and that the indenter slides easily over the surface of the component. This was not observed experimentally, as seen in Figure 25, which shows the predicted deformed plot compared to a photograph of the actual component. The inclusion of friction (friction coefficient = 0.2) in this analysis has a large effect on the predictions. The component is predicted to be able to sustain greater loads, approaching those observed experimentally and now remains upright, rather than collapsing to one side as before, see Figure 26.

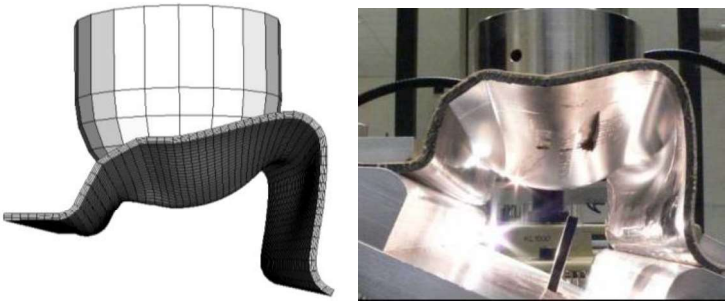

Figure 25. *Comparison of armrest predicted deformed plot obtained from analysis without friction with experimentally observed deformation at 30 mm displacement.*

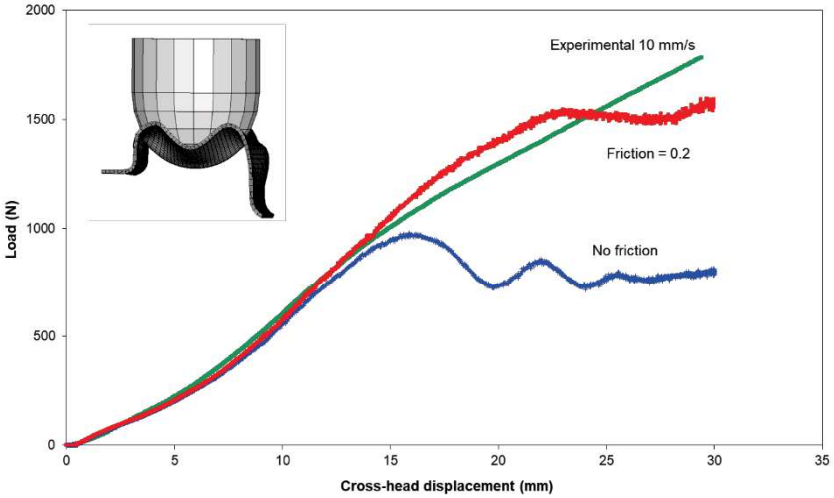

***Figure 26**. Comparison of armrest predicted force-displacement plots run with friction (friction coefficient of 0.2 used) and without friction and experimental data at 10 mm/s.*

Choice of solver

During an FE simulation, the numerical problem defined in an input file is solved using a mathematical code. The FE package Abaqus has a choice of solver codes. The standard (implicit) code can solve a wide range of linear and nonlinear problems. The explicit code is suitable for short, transient dynamic events, such as impact, and is also very efficient for highly nonlinear problems.

In nonlinear analyses the term "convergence" is used to indicate that the solution process for the nonlinear equation system converges. The solution at the end of an increment is, by definition, converged. If the solver cannot find a solution for a given increment of applied load or displacement, another attempt will be made to obtain a converged solution. When a new attempt is made, the solver cuts back the magnitude of the load or displacement increment. Several attempts may be used in any increment of the analysis. If too many attempts are made in a single increment, the solver terminates the analysis – the model has failed to converge.

In the FE package Abaqus, dynamic analyses can be carried out using either the standard (implicit) solver or the explicit solver. The advantage with the standard solver is that the initial time increment size can be chosen manually. The automatic time incrementation scheme

adjusts the increment size as necessary to obtain solutions. This means that the computer processing times are significantly shorter than when using the explicit solver, especially at the lower loading rates. A static analysis is sufficient if only the long-term response of a structure to an applied load is of interest. However, if the duration of the applied load is short, a dynamic analysis should be performed. A dynamic analysis uses an explicit solver and takes account of inertial forces as well as the dependence of yield behaviour on strain rate (rate-dependent plasticity) in the dynamic equation of equilibrium. One limitation of using the explicit solver is that the time step is determined by the time for a stress wave to cross the smallest element dimension. The result is that processing times can be excessive, especially when a refined mesh is being used, or when the analysis is at a low loading rate. The processing time can be reduced by mass scaling i.e. using artificially high values of material density, but care must be taken to ensure that inertial forces still remain insignificant.

EXAMPLE: Mass scaling in dynamic analyses

An example of dynamic analyses of the toptrim component run with different mass scaling factors is shown in Figure 27. Three different mass scaling factors were used. Curve A was obtained using the highest mass scaling factor and doesn't give an accurate prediction. Curve B used a lower mass scaling factor, with an associated increase in computational time. This curve fits the experimental data much better than curve A. Curve C used an even smaller mass scaling factor, with a substantial increase in computational time, but little difference in predicted force-displacement curve. This indicates that the predictions are converging on a steady-state solution and demonstrates that careful use of the mass scaling factor can lead to a reduced analysis time. In this case, the analysis that produced curve B is the best to use, as it gives an accurate prediction within a reasonable time.

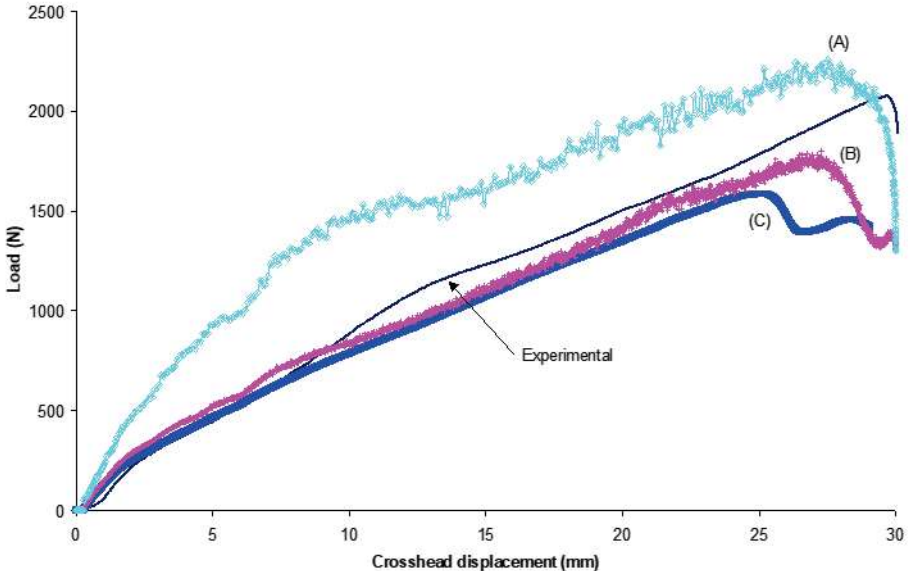

Figure 27. *Example of using three different mass scaling factors in the dynamic analysis of the toptrim component. Curve A used the highest mass scaling factor, curve C used the lowest. Analyses were run with a loading rate of 10 mm/s and are compared to the experimental data.*

Precision level

When using the explicit solver for an analysis with a reasonably slow loading rate, a large number of increments will be required to complete the analysis and it may be necessary to use a double precision executable. Single precision means that the floating point numbers will be represented in 32 bit system whereas double precision means that they will be represented in 64 bit system. The single precision executable typically results in a CPU savings of 20% to 30% compared to the double precision executable, and single precision provides accurate results in most cases. Exceptions in which single precision tends to be inadequate include analyses that require greater than approximately 300,000 increments, have typical nodal displacement increments less than 10–6 times the corresponding nodal coordinate values, include hyperelastic materials, or involve multiple revolutions of deformable parts; here, double precision will be more accurate and is recommended in these cases [5]. Comparison of solutions obtained with single and double precision will indicate the significance of the precision level. If no significant difference is found between single and double precision solutions for a particular model, the single precision executable would be adequate.

EXAMPLE: Single versus double precision

Figure 28 shows the difference between an analysis run with single precision and the same analysis run using double precision. In this case the analysis was of the toptrim component loaded at 0.1 mm/s. As this is a slow loading rate, a high number of increments are required for the explicit analysis. When running the analysis with the default single precision, Abaqus gives a warning message in the data file that a large number of increments will be required and recommends that double precision should be used. It is clear in this case that double precision should be used. The 'double precision' curve shown in Figure 28 is the same basic shape as the 'single precision' one, but much smoother. This is because the use of double precision has removed rounding errors that are present in the single precision analysis.

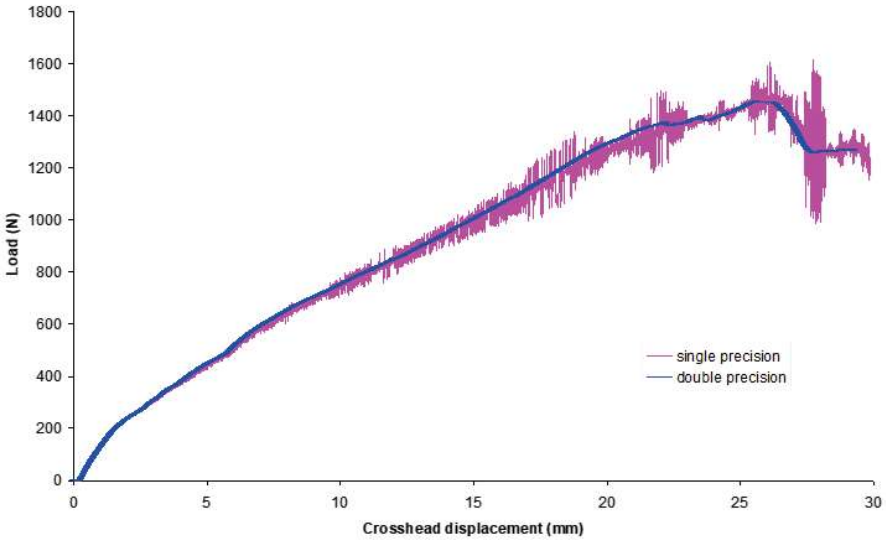

Figure 28. *Comparison of predictions obtained from analyses run using single precision and double precision. Predictions were of the toptrim component loaded at 0.1 mm/s.*

Materials models

Material model selection

The choice of materials model is of great importance when running an FE analysis if the accuracy of predictions in the analysis is important. It affects the accuracy of both the force/displacement curves and the stress and strain predictions. Chapter 2 of this Good Practice Guide provides detailed information on three elastic-plastic materials models: the von Mises and linear Drucker-Prager models are available in most FE packages, whilst the NPL

cavitation model is an extension of the linear Drucker-Prager that includes the effect of material cavitation. Methods for obtaining the necessary materials data have been outlined in Chapter 3, while the calculation of parameters is discussed in Chapter 4. In many situations, the choice of material model will be determined by the material data available. The von Mises model requires the minimum amount of data, needing only Young's modulus, Poisson's ratio and, for a single rate analysis, a hardening curve obtained from a tensile stress strain curve. These data may be available from material databases derived from tests on standard moulded specimens, but it is recommended that specimens of the actual material be tested if possible to obtain the most relevant data. The linear Drucker-Prager and cavitation models require further data, obtained from tests under different stress states e.g. shear, and a greater degree of data manipulation. These requirements increase the quantity of experimental tests necessary, but the use of these models will lead to more accurate predictions of the material behaviour. This is demonstrated in the following example.

EXAMPLE: Comparison of elastic-plastic models

The deformation of the toptrim component (see Figure 22) has been predicted using the von Mises, linear Drucker-Prager and Cavitation elastic-plastic models. The predicted force-displacement curves are compared to experimental data in Figure 29.

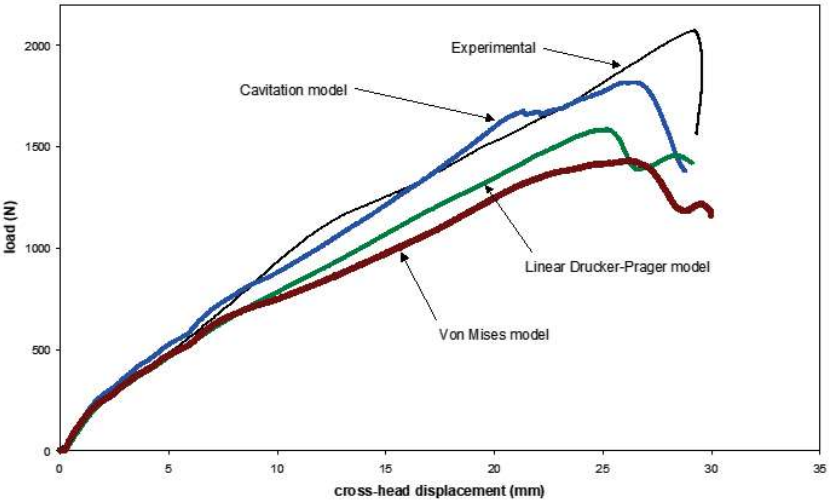

Figure 29. *Comparison of measured force-displacement curve for the toptrim component tested at 10 mm/s with curves predicted using the von Mises, Linear Drucker-Prager and cavitation models.*

As expected, the most basic model, the von Mises, provides the poorest correlation. Use of the linear Drucker-Prager model improves the accuracy of the analysis. The cavitation model matches the experimental data well. For all three analyses maximum principal stresses and strains were obtained at the peak load. The predicted values are presented in Table 7. For this component, the linear Drucker-Prager and cavitation models predict similar stress and strain values. The von Mises model, however, predicts a higher maximum principal stress and a much lower strain value, demonstrating the inaccuracy of this model.

Materials model	Maximum principal stress (MPa)	Maximum principal true strain
Von Mises	26.8	0.047
Linear Drucker-Prager	23.60	0.076
Cavitation	22.9	0.08

Table 7. *Maximum Principal Stress and Strain predicted by three elastic-plastic models at the peak load, for the toptrim component.*

Rate-dependent behaviour

Whichever model is used for a stress analysis, more accurate predictions will be made if the dependence of properties on strain rate is taken into consideration. Many finite element packages have the ability to include the dependence of yield behaviour on strain rate (rate-dependent plasticity) by including a series of hardening curves measured at different strain rates. Information on the determination of hardening curves is given in Chapter 4 along with a procedure for determining properties at high strain rates by modelling tensile hardening curves measured at slower speeds and determining the dependence of parameters on strain rate and calculating the curves at higher strain rates by extrapolation. The example below demonstrates the difference between predictions obtained with rate-dependent and rate-independent analyses.

EXAMPLE: Comparison of single rate and rate-dependent analyses

In this example rate-independent (single-rate) analyses have been carried out on the armrest component using the linear Drucker-Prager model. Low-rate hardening curves (approximately 0.001 s^{-1}) are the easiest to measure, so a single-rate analysis was run with one of these hardening curves. A second single-rate analysis was carried out using a hardening curve at 0.15 s^{-1} that was thought to be more appropriate to the actual test conditions. Predictions from these analyses are compared with the force-displacement curve predicted in a rate-

dependent analysis in Figure 30. The rate-dependent analysis was run using the suite of tensile hardening curves shown in Figure 15.

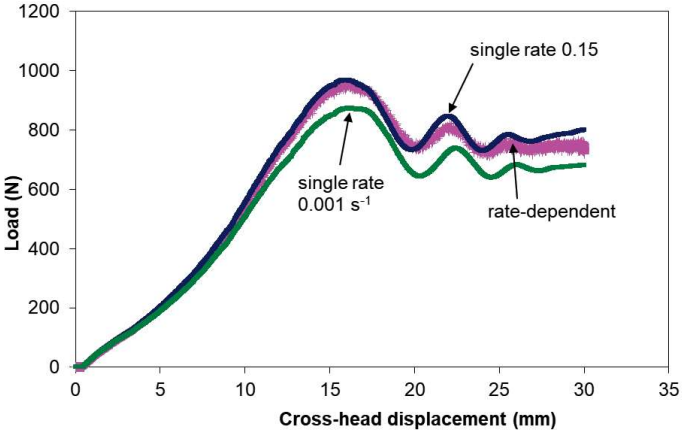

Figure 30. *Comparison of single-rate and rate dependent analyses run with the linear Drucker-Prager model at 10 mm/s compared with measured data.*

The use of a low-rate curve underestimates the peak loads in the component. When more care is taken in selecting an appropriate single rate curve, then reasonable predictions can be obtained. As it is difficult to estimate the varying strain rates within a complex shape during impact loading, it is always prudent to include rate-dependent data if possible. The accuracy of strain predictions is considered to be higher if a dynamic analysis is undertaken with rate-dependent hardening data i.e. multiple hardening curves, rather than a single strain rate hardening curve. This is because strain localisation, which is caused by enhanced softening of the adhesive in regions of high strain, is alleviated with rate-dependent data. This arises because the regions of high strain are also subjected to high strain rates, which increase the yield stress and reduce the strain softening associated with rate-independent yielding.

The maximum principal stresses and strains have been studied at the peak loads (approximately 15 mm displacement). Values were obtained from central elements directly underneath the indenter and are presented in Table 8. The low strain rate hardening curve (0.001 s^{-1}) predicts a stress that is much lower than that obtained from the rate-dependent analysis, and a strain prediction which is higher. The carefully chosen single strain rate curve (0.15 s^{-1}) predicts stress and strain values that are approaching those predicted with the rate-dependent analysis although stresses and strain predictions may be more dissimilar at regions of high strain.

Materials model	Maximum principal stress (MPa)	Maximum principal true strain
Rate-dependent	21.0	0.051
Single rate (0.001 s^{-1})	18.2	0.057
Single rate (0.15 s^{-1})	23.5	0.053

Table 8. *Maximum Principal Stress and Strain predicted by three elastic-plastic models at the peak load, for the armrest component.*

Parameter sensitivity

Chapter 4 of this Good Practice Guide covers the determination of parameters for the cavitation model. Table 9 demonstrates the number of parameters that are required to use the cavitation model. Some may be broadly independent of polymer type (q1 and μ_1'), while others need to be measured. Some of these measured values are consistent with those used in other elastic-plastic models (E, ν^e), while others are unique to the cavitation model. Any parameter obtained from measured data has a degree of uncertainty attached to it. When data are required from tests under two stress states, for example in the calculation of μ, it is likely that the parameter value will depend upon which pair of data points is selected [15]. Sensitivity analyses can be undertaken to get a feel for the effect of these parameters on the prediction obtained. An example of a small sensitivity analysis is presented below. A full-scale parametric study has not been carried out. Instead, the parameters have been individually changed to values that roughly correlate to the uncertainty in the measured value.

EXAMPLE: Cavitation model parameter sensitivity

As the cavitation model requires the greatest number of parameters this model was used to investigate parameter sensitivity. One armrest analysis was run at 10 mm/s using a full set of cavitation model parameters that had been obtained from data at 0.01 s^{-1}. These parameters are shown in Table 9 and are described briefly in Chapter 4. Six further analyses were then run, each having a single parameter changed except in the case of the parameters σ_{ofo} and C, which are used to define the effective shear flow stress and its dependence on strain rate (see equation (32)) and were changed together. The new values used for each of these parameters are also shown in Table 9.

Parameter	0.01 s^{-1} data	New values
E (GPa)	1.78	2.45
ν^e	0.37	
μ	0.36	0.3
v_C	0.4	0.45
k	2.5	
q_1	1.5	1.58
μ_1'	0.13	0.17
ε_{1v}	0.003	
ε_{2v}	0.01	
β	0.9	
σ_{ofo}	35.9	28.7
C	3.9	3.1

Table 9. *Values for parameters in the cavitation model at a strain rate of 0.01 s^{-1}*

Figure 31 reveals that changes in the parameters μ, v_C, q_1 and μ_1' have no significant effect on the predicted force-displacement curves. The parameters σ_{ofo} and C are responsible for the rate-dependence calculations within the model, where σ_{ofo} is the flow stress. Lowering σ_{ofo} and C is seen to significantly reduce the peak load predicted. From this set of analyses, it appears that the Young's modulus has a large effect on the force-displacement plots. The modulus had been increased to 2.45 GPa (a typical value obtained from data tested at a strain rate of 10 s^{-1}) and this produced a predicted force-displacement curve that was much higher than all the other curves in Figure 31. This indicates that rate-dependent elasticity could have a place in these analyses.

The predicted maximum principal stress and strain values were obtained for the two cases that produced significantly different force-displacement curves. Values were obtained from central elements directly underneath the indenter at the peak loads (approximately 15 mm displacement) and are presented in Table 10. The results show that although changing the modulus raises the peak load observed, the actual stresses and strains predicted in the region analysed were very similar to those obtained in analysis using the original 0.01s^{-1} data. In contrast, lowering the rate-dependence parameters has had a significant effect on the predicted stress, although the strain level remains similar.

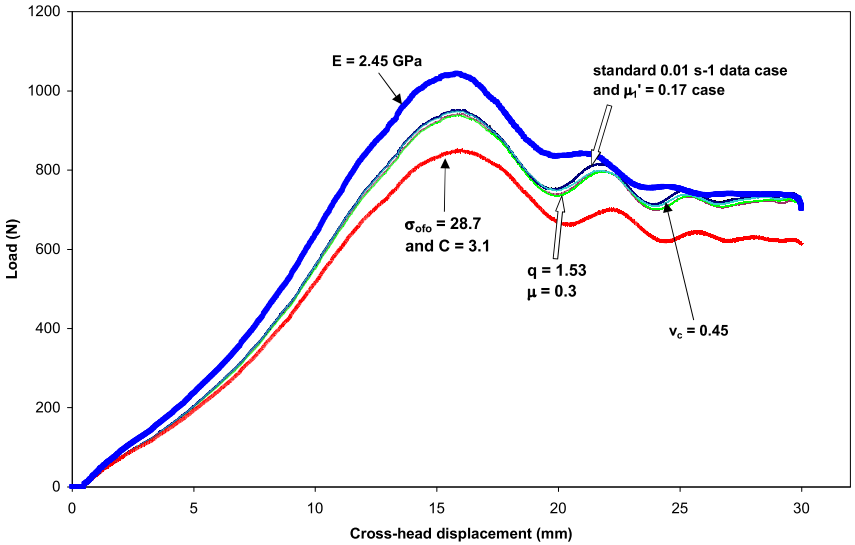

Figure 31. *Force-displacement curves predicted using cavitation model as part of sensitivity analyses. One analysis was run with 0.01 s^{-1} data. Subsequent analyses had a single parameter changed.*

Changed Cavitation Model Parameter	Maximum principal stress (MPa)	Maximum principal true strain
Original 0.01s^{-1} data	21.0	0.051
Increase modulus	21.2	0.054
Decreased rate-dependence parameters	16.3	0.054

Table 10. *Maximum Principal Stress and Strain predicted by cavitation model with different input parameters, for the armrest component at the peak load.*

This example highlights the need to have an understanding of the sensitivity of parameters. It emphasizes the need to have accurate Young's modulus data and demonstrates that some parameters may not be very sensitive to change. For the insensitive parameters it may be reasonable to use one value for a range of polymers, but this is not an assumption that should be made without any exploration of the sensitivity.

Predicting performance

Finite element analysis (FEA) is a very useful aid in the prediction of plastics performance under impact. As shown in the previous examples, an analysis enables the deformation of a component to be predicted together with distributions of stress and strain within the component. Tough plastics have characteristic properties that make them particularly suited to applications where accidental impact loading is possible, such as components in motor vehicles where the material must withstand the impact without failure or must limit the force level sustained by the passenger. The ability to predict the response of a plastics product under impact loading is therefore an important aspect of the design of these products in order to optimise safety and reliability in their performance. The following examples show the effectiveness of using FEA to predict the deformation behaviour of a component.

EXAMPLE: Predicting deformation of the toptrim component

In this example, the toptrim component (Figure 22(a)) has been used. The experimental test set-up was such that a camera could be used to photograph the specimen during testing. The toptrim component was indented with a hemispherical indenter at a rate of 0.1 mm/s. Photographs were taken every 10 seconds to monitor the degree of component deformation. Force-displacement data were also obtained. A comparative FE analysis was run using the cavitation model.

It can be seen from Figure 32 that the predicted force-displacement values match the experimental data reasonably well. The photographs taken during testing were used to validate the FE predictions, by comparing them to the predicted deformed plots. An example is shown in Figure 33, which compares the photograph and deformed plot (Figure 33(a)) obtained at an indenter displacement of 20 mm. The FE prediction correlates well with the experimental deformation, with deformation only occurring in the central two ribs. To illustrate a less accurate prediction the deformed plot obtained from the linear Drucker-Prager analysis is also presented (Figure 33(b)). In this case the model is predicting deformation of the central two ribs plus deformation in the next pair of ribs, which isn't observed experimentally.

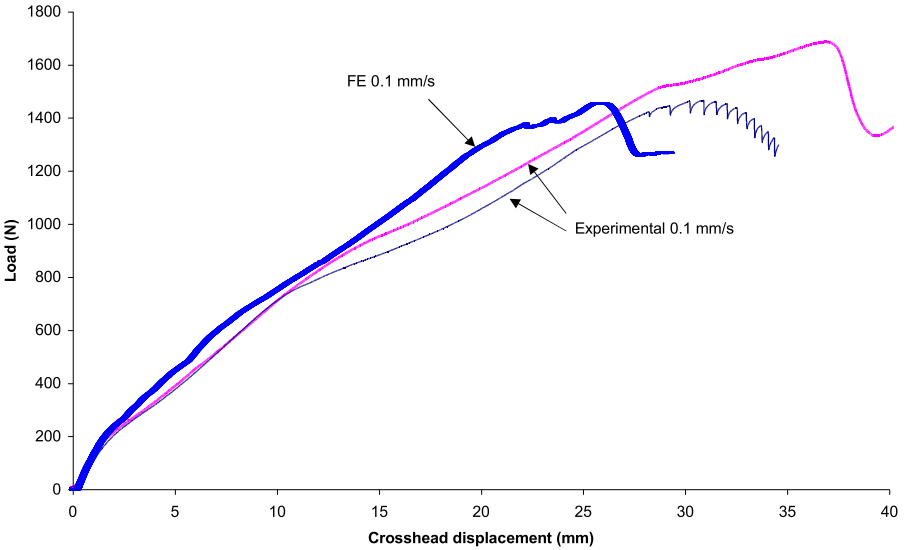

Figure 32. *Comparison of experimental and predicted force-displacement curves obtained from the toptrim component at a loading rate of 0.1 mm/s.*

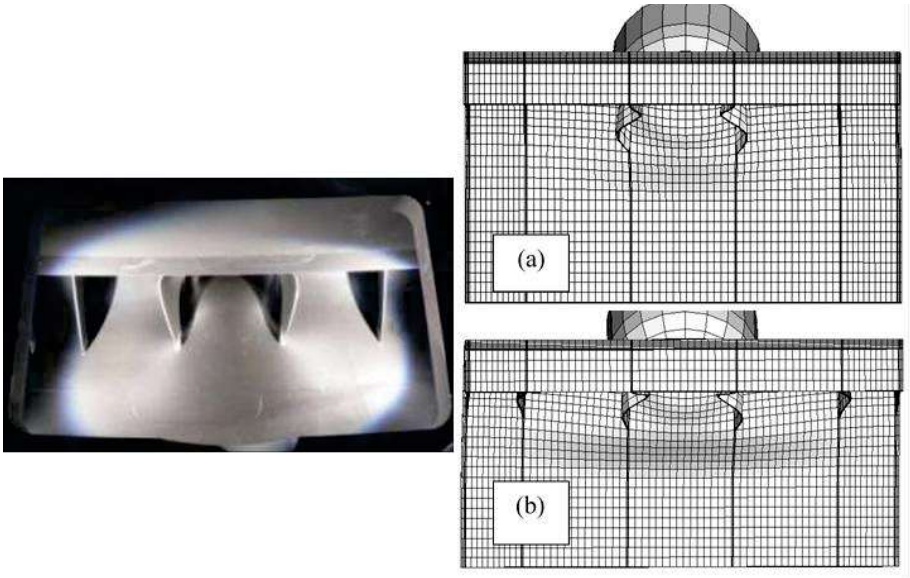

Figure 33. *Photograph of toptrim component taken during testing, at a displacement of 20 mm, compared with FE predictions obtained at the same displacement using (a) cavitation model and (b) linear Drucker-Prager model.*

EXAMPLE: Optimisation of components

Finite element analysis enables the optimisation of components without lengthy experimental test schedules as the influence of factors such as geometry, loading etc can be rapidly and easily explored. For instance, FE could be used to investigate the effect of different indenter shapes, see Figure 34. This figure presents the predicted force-displacement curves obtained using spherical and cylindrical indenters and shows a marked difference in response from the two indenters.

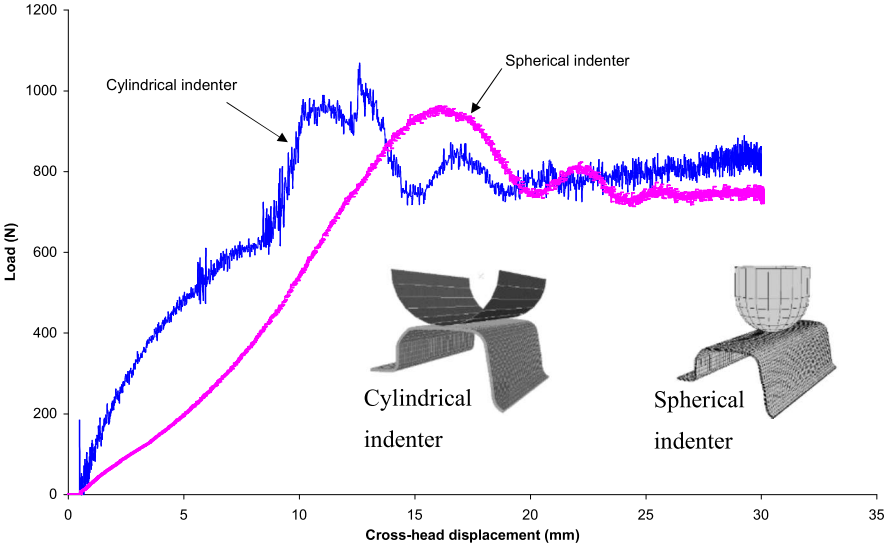

Figure 34. *Force-displacement curves predicted from indentation of the armrest component with spherical and cylindrical indenters.*

FE can also be used to investigate how sensitive components are to impact location. During a vehicle collision, passenger impact may occur anywhere along the component parts shown in Figure 22. The toptrim component has been studied using the linear Drucker-Prager analysis, with impact occurring at several different locations. The indenter was set to impact at the midpoint between the two central ribs; directly above a rib and at two locations between these two. There is a large difference between the results at small displacements, see Figure 35. The component response is much stiffer when impact occurs above a rib. By a cross-head displacement of 7 mm, the four force/displacement curves have aligned. The curves that showed the highest initial stiffness have slightly lower maximum loads. This method of

exploring geometry and loading factors is clearly much faster and cheaper than the equivalent experimental investigation.

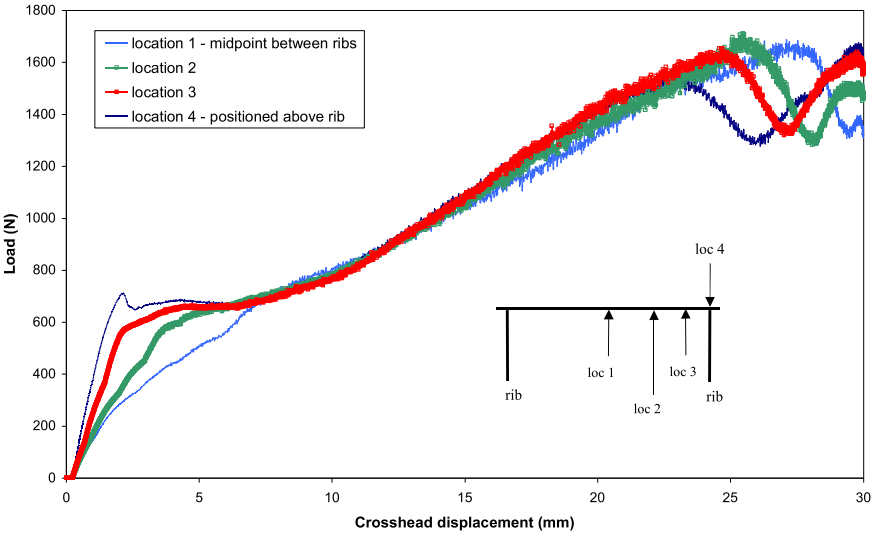

Figure 35. *Toptrim force-displacement plots obtained when indenter impacts at 4 different locations.*

Chapter 6

Conclusions

Conclusions

Finite element systems use elastic-plastic models to describe the non-linear, large-strain behaviour of rigid materials. Although not developed for plastics materials, these models can be used to predict forces and deformations associated with a component under impact loading. The accuracy of predictions will depend on the suitability of the model for the polymer being studied and the accuracy achieved in the determination of model parameters.

The elastic-plastic model based on the von Mises yield criterion is the simplest model but neglects any influence of the hydrostatic component of stress on yield behaviour. The data requirements for this model can be derived from tensile tests alone and are a Young's modulus, a Poisson's ratio and tensile hardening curves. Since the yield behaviour of plastics depends on strain rate, for maximum accuracy in predictions, these curves should be determined over a range of strain rates relevant to the application. Tensile hardening curves are shown in Figure 15 and can be modelled using equations (28) and (29).

Values for Young's modulus and Poisson's ratio are given in Table 1 at a strain rate of 0.01 s^{-1}. The Young's modulus will increase with strain rate, and a higher value should ideally be used for impact simulations. Whilst the variation of tensile modulus with strain rate could be obtained by analysis of the tensile curves in Figure 13, it should be noted that the gauge length of the extensometer used for the acquisition of these data was 4 mm. Accurate modulus measurements at higher strain rates should be determined from tests using the ISO specimen where a larger gauge length can be used (Chapter 3).

The linear Drucker-Prager model is more accurate for plastics than the von Mises model since it accounts for some influence of the hydrostatic component of stress on yield behaviour. Determination of the parameters for this model requires data from tests in tension and one other stress state such as shear or compression. Whilst this model accounts for different yield stresses in tension and compression, it is not possible to accurately predict stress/strain behaviour, under shear and compression, and Poisson's ratio for materials that exhibit significant cavitation (void formation) under tensile stress states. Values for the parameters in the linear Drucker-Prager model are given in Table 1 at a low strain rate. The shape of the hardening curve and its variation with strain rate can be modelled using equations (28) and (29). Values for the parameters in these equations are given in Table 4.

The cavitation model takes account of the nucleation of cavities on yield behaviour under stress states where there is a significant hydrostatic component. Cavities nucleate in the more mobile regions of the polymer, which in the materials studied here are presumably the amorphous phase and the rubber toughening particles. Debonding at the interface with filler particles may also contribute to the overall effective volume fraction of voids. The nucleation of cavities is assumed to be determined by the level of volumetric strain and to take place over a range of volumetric strain for a distribution in the size of the mobile regions. Values for the parameters in the cavitation model are given in Table 2 at a low strain rate. The hardening behaviour in this model is characterised by the effective shear stress against effective shear plastic strain curve. The variation in hardening behaviour with strain and strain rate is given by equations (31) and (32) with the parameter values listed in Table 5. Experimental data over a range of strain rate indicate that the parameter v_C varies slowly with strain rate.

The variation of modulus with strain rate can be investigated using a linear viscoelastic analysis (see Chapter 4) with experimental stress relaxation data. This analysis demonstrates that the concept of a Young's modulus is ambiguous for a viscoelastic material.

There are many decisions to be made when setting up an FE model, such as element type, material model selection and analysis type. This Good Practice Guide discussed some of the options available such as the use of different element types (solid and shell); different analysis types (rate-dependent, rate-independent); mass scaling; precision level; modelling contact and the influence of friction. Examples of these options are provided.

Comparisons of predictions from the three models discussed in this Guide are presented. When compared to the cavitation model, the linear Drucker-Prager was found, for the cases investigated, to be adequate despite the simplifying assumptions, although stress and strain predictions may be dissimilar at regions of high strain. The von Mises model gave the least accurate predictions of component behaviour. For reliable predictions, accurate materials parameters must be used. This has been the focus of sensitivity analyses, which have been carried out to indicate how sensitive predictions are to changes in the cavitation model parameters. In this study modulus and flow stress (σ_{ofo}) were found to be the most influential materials parameters in the cavitation model. In the small region of elements studied, changing modulus had little effect on predicted stress and strain values, while changing the flow stress caused a significant change in predicted stress.

Chapter 7

References

References

1. C. B. Bucknall: in ' The Physics of Glassy Polymers', ed. by R. N. Haward and R. J. Young, 2nd edn., ch.8, 1997, Chapman and Hall.
2. ISO 527-2, Plastics – Determination of tensile properties – Part 2: Test conditions for moulding and extrusion plastics.
3. I. M. Ward: in 'Mechanical Properties of Solid Polymers', 2nd edn, ch.11, 1983, John Wiley and Sons, Ltd.
4. B. Crist: in ' The Physics of Glassy Polymers', ed. by R. N. Haward and R. J. Young, 2nd edn., ch.4, 1997, Chapman and Hall.
5. Abaqus 2021 user documentation, © 2009-2021, Dassault Systèmes Simulia Corp
6. G Dean and L Crocker. Plastics, Rubbers and Composites, Vol 36, No 1, Feb 2007, pp1-13; https://doi.org/10.1179/174328907X174575
7. L Crocker and G Dean. Plastics, Rubbers and Composites, Vol 36, No 1, Feb 2007, pp14-25; https://doi.org/10.1179/174328907X174584
8. A. Gurson. J. Eng. Mater. Technol., Trans ASME, (1977), 99, p 2.
9. V, Tvergaard. Int. J. Fract. Mech., (1981), 17, p 389.
10. A. Lazzeri and C. Bucknall. J. Mat. Sci., (1993), 28, p 6799.
11. B. Read and G. Dean. Plastics, Rubber and Composites, (2001), 30, p 328.
12. G. Dean, B. Read and L. Wright. NPL Report MATC(A)120, September 2002
13. M. Arcan, Z. Hashin and A. Voloshin. Exp. Mech., (1978), 18, 141
14. G. Dean, L. Crocker, B. Read and L. Wright. Int. J. Adhesion and Adhesives, (2004), 24, 295
15. G Dean and L Crocker, NPL Report DEPC-MPR 043, February 2006